

# A FULLY ITERATIVE ADAPTIVE ENERGY-BASED APPROACH FOR MONOTONE ELLIPTIC PROBLEMS

RAPHAEL LEU AND THOMAS P. WIHLER

**ABSTRACT.** We present a fully iterative adaptive algorithm for the numerical minimization of strongly convex energy functionals in Hilbert spaces. The proposed approach, which we first present in abstract form, generates a hierarchical sequence of adaptively refined finite-dimensional approximation spaces and employs a (nonlinear) conjugate gradient (CG) method to compute suitable approximations on each space. A core novelty of our approach is that all components of the algorithm are consistently driven by *energy reduction principles* rather than by classical a posteriori estimators. In particular, adaptive refinement is steered by local energy reduction indicators which aim to construct subsequent approximation spaces in a way that attains the largest potential decrease in energy. Likewise, the stopping criteria for the iterative solver are based on either relative or averaged energy reductions on each subspace. As a concrete realization, we present a concise implementation for  $\mathbb{P}_1$  finite element discretizations of second-order semilinear elliptic diffusion-reaction models, where the local indicators driving the element refinements are computed based on edge-wise energy reductions. Numerical experiments demonstrate that the resulting scheme achieves optimal convergence for various benchmark problems in two-dimensional polygonal domains.

## 1. INTRODUCTION

We study the numerical minimization of energy functionals  $\mathbf{E} : \mathbb{V} \rightarrow \mathbb{R}$  defined on a Hilbert space  $\mathbb{V}$  with inner product  $(\cdot, \cdot)_{\mathbb{V}} : \mathbb{V} \times \mathbb{V} \rightarrow \mathbb{R}$  and induced norm  $\|v\|_{\mathbb{V}} := \sqrt{(v, v)_{\mathbb{V}}}$ . Throughout, we assume the following:

*Assumption 1.* The energy functional  $\mathbf{E} : \mathbb{V} \rightarrow \mathbb{R}$  is

- (i) *Gâteaux differentiable*, with the derivative denoted by  $\mathbf{E}' : \mathbb{V} \rightarrow \mathbb{V}'$ ,  $u \mapsto \mathbf{E}'[u]$ , where  $\mathbb{V}'$  signifies the dual space of  $\mathbb{V}$ ;
- (ii) *weakly coercive*, i.e.  $\mathbf{E}(v) \rightarrow +\infty$  as  $\|v\|_{\mathbb{V}} \rightarrow \infty$ ;
- (iii) *strictly convex*, i.e.  $\mathbf{E}(tu + (1-t)v) < t\mathbf{E}(u) + (1-t)\mathbf{E}(v)$  for any  $t \in (0, 1)$  and for all  $u, v \in \mathbb{V}$  with  $u \neq v$ .

Under these assumptions, standard arguments of variational calculus yield the existence of a unique minimizer  $u \in \mathbb{V}$  of  $\mathbf{E}$ , i.e.

$$\mathbf{E}(u) < \mathbf{E}(v) \quad \forall v \in \mathbb{V}, v \neq u, \quad (1.1)$$

which, for Gâteaux differentiable functionals, is equivalently characterized by the weak formulation

$$\mathbf{E}'[u](v) = 0 \quad \forall v \in \mathbb{V}, \quad (1.2)$$

see [Zei90, Cor. 25.18]. We refer to the solution of (1.2) as the *full space solution*. Clearly, all properties of Assumption 1 carry over to any finite-dimensional (and thus closed) subspace  $\mathbb{W} \subset \mathbb{V}$ ; in particular, the unique minimizer  $u_{\mathbb{W}} \in \mathbb{W}$  of  $\mathbf{E}$  over  $\mathbb{W}$  exists and satisfies

$$\mathbf{E}'[u_{\mathbb{W}}](w) = 0 \quad \forall w \in \mathbb{W}. \quad (1.3)$$

We call the solution of (1.3) the *Galerkin solution in  $\mathbb{W}$* .

---

MATHEMATICS INSTITUTE, UNIVERSITY OF BERN, CH-3012 SWITZERLAND

2020 *Mathematics Subject Classification.* 35A15, 35B38, 65J15, 65M50, 65N30.

*Key words and phrases.* Adaptive finite element methods, energy-based algorithms, iterative energy reduction schemes, energy minimization, iterative linearized Galerkin methods, conjugated gradient method, variational adaptivity, adaptive mesh refinements, monotone elliptic boundary value problems.

The authors acknowledge the support of the Swiss National Science Foundation, Grant No. 200021.212868.

Energy minimization problems satisfying Assumption 1 naturally arise in the context of linear and nonlinear monotone elliptic partial differential equations (PDEs) of variational type; more specifically, for the purpose of the numerical experiments in the present work (see Section 4), we shall focus on semilinear diffusion-reaction boundary value problems in divergence form, with monotone reaction terms, cf. (4.1).

**Adaptive FEM and ILG approach.** The application of adaptive finite element methods (AFEM) for the numerical approximation of weak formulations (1.2) in the context of elliptic (and parabolic) PDE is well established, whereby they typically follow the classical `solve-estimate-mark-refine` paradigm: on a given finite element mesh, the Galerkin solution is computed (or an inexact approximation thereof), and a posteriori (residual or error) estimators are employed to flag elements for local refinement.

In the so-called iterative linearized Galerkin (ILG) methodology, see, e.g. [HW20], the weak formulation (1.2) is solved numerically based on an instantaneous interplay of iterative solvers (which deal with possible nonlinearities or with linear solver errors resulting from the approximation of the algebraic systems) with local mesh enrichments. In combination with AFEM, this approach starts from an initial finite-dimensional subspace  $\mathbb{V}_0 \subset \mathbb{V}$ , which is adaptively refined to construct a nested sequence of subspaces  $\mathbb{V}_0 \subset \mathbb{V}_1 \subset \dots \subset \mathbb{V}_N \subset \dots \subset \mathbb{V}$ . On each space  $\mathbb{V}_N$ ,  $N \geq 0$ , the corresponding Galerkin solution (i.e. the solution of (1.3) on  $\mathbb{W} = \mathbb{V}_N$ ), denoted by  $u_N^h \in \mathbb{V}_N$ , is approximated by a sequence of approximations  $\{u_N^n\}_n \subset \mathbb{V}_N$  that results from the application of iterative (nonlinear or linear) solvers. In practice, the iteration is stopped after finitely many steps, yielding a final iterate  $u_N^* \in \mathbb{V}_N$  for each subspace. From a theoretical point of view, this process is typically controlled by decomposing the error into two contributions (in the simplest case), viz.

$$u - u_N^* = (u - u_N^h) + (u_N^h - u_N^*),$$

where the two brackets on the right-hand side contain the *discretization error* and the *iteration error*, respectively, with the full-space solution  $u \in \mathbb{V}$  of (1.2). Correspondingly, in the ILG approach, the overall error is optimally bounded by balancing both the discretization and iteration errors, whereby the latter depends on both the (linear or nonlinear) solvers employed as well as on the stopping criterion used to select the final iterate  $u_N^* \in \mathbb{V}_N$ . Within an iterative adaptive context, controlling the total error therefore requires careful monitoring of all three of these key components, which is typically accomplished by deriving suitable a posteriori estimates that are able to account individually for each of these error sources. We refer to the works [CW17; HPW21; HW20] on the ILG approach, or the related works [Bec+23; BPS25; EV13; Hab+21; JSV10] for further details.

**Variational adaptivity.** Notably, the AFEM approach usually does *not* explicitly exploit a possible energy structure of the PDE problem under consideration, which is in contrast to the recent *variational adaptivity* methodology, see [AHW23; HSW21; HW25], to be further developed in the current article; we also mention the paper [Har+24] for energy-related a posteriori bounds. Indeed, in this new approach, all algorithmic components are motivated and guided by *energy minimization principles*. Here, we may bear in mind that both the full-space solution  $u \in \mathbb{V}$  of (1.2) and the Galerkin solution  $u_N^h \in \mathbb{V}_N$  from (1.3) are equivalently characterized as the unique energy minimizers over their respective spaces, cf. (1.1). We will demonstrate in the present paper that this observation allows to address the above-mentioned error components using techniques inspired by (variational) principles of energy reduction, which, crucially, do not rely on classical a posteriori error estimates. Thereby, this novel avenue proves to be a widely applicable framework for the efficient practical approximation of linear and nonlinear PDE, where such bounds are unavailable or difficult to obtain.

In the context of finite element discretizations, variational adaptivity replaces the local (residual-based) error estimation step by a local energy reduction prediction. These indicators quantify potential energy reductions induced by using additional degrees of freedom that locally enrich the current approximation space. This idea applies in very general terms to essentially any variational problem that involves operators with a local structure, and to a broad class of (conforming)

numerical methods: For instance, for  $hp$ -type finite element methods for (self-adjoint) linear and nonlinear elliptic PDE, the local enrichment corresponding to an increase in the local polynomial degree or a local mesh refinement may, in both cases, be realized in a highly effective way by adding suitable local degrees of freedom; see [BSW25] and [Hei+25] for linear elliptic PDE or for linear and nonlinear eigenvalue problems, respectively.

**Contribution.** Compared to the available papers on variational adaptivity [AHW23; HSW21; HW25], where the Galerkin solution is obtained by repeatedly linearizing the nonlinear problem and by dealing with the resulting large-scale linear systems with the aid of direct solvers, the present work advances this line of research by proposing a *purely iterative energy-based method* in which the arising discrete problems are no longer solved exactly. Instead, we compute inexact solutions employing a (nonlinear) conjugate gradient (CG) method in conjunction with suitable energy-based stopping criteria.

To illustrate our approach, we present a novel realization of variational adaptivity for  $\mathbb{P}_1$  finite element discretizations in two space dimensions. In this context, the works [AHW23; HSW21; HW25] have used local red refinement of individual (triangular) elements in 2d to compute energy reduction indicators. In contrast, we propose an even more local *edge-based variational adaptivity strategy*, where potential energy reductions are associated with element interface edges, and realized through edge bisection. This yields a more efficient and elegant algorithm: Firstly, in contrast to element-based refinement, each edge (or face) is refined only once during the marking step; secondly, the resulting local linearized problems admit simple closed-form solutions. Finally, we numerically demonstrate that variational adaptivity retains optimal convergence rates for the sequence of final iterates, even when no large-scale linear system is solved exactly.

**Outline.** The remainder of this paper is organized as follows: In Section 2, we begin by considering the case where the energy  $\mathbf{E}$  in (1.1) is linear-quadratic; this permits to motivate both the CG method as a natural iterative solver for convex variational problems and the introduction of two different energy-oriented stopping criteria for the CG scheme. Furthermore, we highlight some key properties relevant for its interpretation as an energy minimization method. Section 3 introduces the concept of variational adaptivity, which is first presented as an abstract, energy-driven space enrichment strategy used to generate a sequence of hierarchical subspaces based on (local) energy reduction indicators. Subsequently, a concrete realization of this framework in the context of finite element discretizations is developed; in particular, we propose an edge-based variational adaptivity strategy that may be viewed as a straightforward yet highly effective realization of the abstract approach. Finally, Section 4 presents a series of numerical experiments assessing the performance of the overall method. We report on convergence behavior and demonstrate the effectiveness of variational adaptivity within a fully iterative, inexact-solver setting.

## 2. ITERATIVE SOLVER AND STOPPING CRITERIA

In this Section, we introduce the iterative solver and the associated stopping criteria for the numerical solution of (1.3) on a fixed finite-dimensional subspace. To this end, we first consider the problem in a simplified setting. We then conclude that the strategy presented below naturally extends to more general energy minimization problems.

**2.1. A Simplified Model Problem.** For the sake of this discussion, we temporarily assume that  $\mathbf{E} : \mathbb{V} \rightarrow \mathbb{R}$  is *linear-quadratic*, i.e. of the form

$$\mathbf{E}(v) = \frac{1}{2}a(v, v) - \ell(v), \quad (2.1)$$

where  $a : \mathbb{V} \times \mathbb{V} \rightarrow \mathbb{R}$  is a bounded, coercive, and symmetric bilinear form, inducing an inner product  $(v, w)_a := a(v, w)$  on  $\mathbb{V}$  with corresponding *energy norm*  $\|v\|_a := \sqrt{(v, v)_a}$ , and  $\ell : \mathbb{V} \rightarrow \mathbb{R}$  denotes a bounded linear functional. In this setting,  $\mathbf{E}$  satisfies Assumption 1. Therefore, there exists a unique minimizer  $u \in \mathbb{V}$  of  $\mathbf{E}$  which is equivalently characterized by the weak formulation

$$\mathbf{E}'[u](v) = a(u, v) - \ell(v) = 0 \quad \forall v \in \mathbb{V}. \quad (2.2)$$

Again, all properties of  $\mathbf{E}$  carry over to any (finite-dimensional) linear subspace  $\mathbb{W} \subset \mathbb{V}$  and hence,  $\mathbf{E}$  admits a unique minimizer  $u_{\mathbb{W}} \in \mathbb{W}$  over the space  $\mathbb{W}$  that is equivalently characterized by the weak form

$$\mathbf{E}'[u_{\mathbb{W}}](w) = a(u_{\mathbb{W}}, w) - \ell(w) = 0 \quad \forall w \in \mathbb{W}. \quad (2.3)$$

The following lemma will be instrumental in the sequel.

**Lemma 1.** *Let  $\mathbb{W} \subset \mathbb{V}$  be any linear subspace, and  $u_{\mathbb{W}} \in \mathbb{W}$  the unique minimizer of  $\mathbf{E}$  over  $\mathbb{W}$ . Then, for all  $w \in \mathbb{W}$ , the identity*

$$\|u_{\mathbb{W}} - w\|_a^2 = \|u_{\mathbb{W}}\|_a^2 + 2\mathbf{E}(w) \quad (2.4)$$

holds true. Further, setting  $w = u_{\mathbb{W}}$  in (2.4) immediately yields

$$\mathbf{E}(u_{\mathbb{W}}) = -\frac{1}{2}\|u_{\mathbb{W}}\|_a^2 \leq 0,$$

i.e. the energy of  $u_{\mathbb{W}}$  is necessarily non-positive.

*Proof.* Applying the symmetry of  $a(\cdot, \cdot)$ , for any  $w \in \mathbb{W}$ , we infer that

$$\|u_{\mathbb{W}} - w\|_a^2 = a(u_{\mathbb{W}} - w, u_{\mathbb{W}} - w) = a(u_{\mathbb{W}}, u_{\mathbb{W}}) - 2a(u_{\mathbb{W}}, w) + a(w, w).$$

Using that  $u_{\mathbb{W}}$  solves (2.3), we obtain

$$\|u_{\mathbb{W}} - w\|_a^2 = \|u_{\mathbb{W}}\|_a^2 - 2\ell(w) + a(w, w) = \|u_{\mathbb{W}}\|_a^2 + 2\mathbf{E}(w),$$

which completes the argument.  $\square$

**2.2. Galerkin Discretization.** From now on, let  $\mathbb{V}_N \subset \mathbb{V}$  be an  $N$ -dimensional linear subspace and  $\mathcal{B}_N := \{\phi_1, \dots, \phi_N\} \subset \mathbb{V}_N$  a basis of  $\mathbb{V}_N$ . By  $u_N^h \in \mathbb{V}_N$  we denote the unique minimizer of  $\mathbf{E}$  over  $\mathbb{V}_N$ . In this finite-dimensional setting,  $u_N^h \in \mathbb{V}_N$  can be written as

$$u_N^h = \sum_{k=1}^N (\mathbf{U}_N^h)_k \phi_k, \quad (2.5)$$

where  $(\mathbf{U}_N^h)_k \in \mathbb{R}$ ,  $k = 1, \dots, N$ , denote the entries of the coefficient vector  $\mathbf{U}_N^h \in \mathbb{R}^N$ . Defining the stiffness matrix  $\mathbf{A} \in \mathbb{R}^{N \times N}$  and the load vector  $\mathbf{b} \in \mathbb{R}^N$  by

$$\mathbf{A}_{ij} := a(\phi_i, \phi_j) \quad \text{and} \quad \mathbf{b}_j := \ell(\phi_j), \quad 1 \leq i, j \leq N,$$

respectively, the discrete weak formulation (2.3) with  $\mathbb{W} = \mathbb{V}_N$  is equivalent to the linear system

$$\mathbf{A} \mathbf{U}_N^h = \mathbf{b}, \quad (2.6)$$

where  $\mathbf{A}$  is symmetric positive-definite (SPD).

*Remark 1.* The solution of (2.6) may, in principle, be computed using a direct solver. However, for the purpose of the current work, we take into account the case where the space dimension  $N$  becomes large enough to motivate the use of an iterative linear solver; in the context of finite element discretizations, this may become useful or even necessary, for instance, if strongly refined finite element meshes (in particular, in space dimensions  $d \geq 2$ ) are involved, or if higher-order approximations are applied.

**2.3. Iterative Solver.** As motivated in Remark 1, this subsection considers the numerical approximation of  $u_N^h \in \mathbb{V}_N$  by generating an energy minimizing sequence  $\{u_N^n\}_n \subset \mathbb{V}_N$ . Recalling the linear algebra formulation (2.6) with  $\mathbf{A}$  SPD, it is natural to employ the CG algorithm. Then, the  $n$ -th element of this sequence may be written as

$$u_N^n = u_N^0 + \sum_{\ell=1}^n p_N^\ell,$$

where  $u_N^0 \in \mathbb{V}_N$  is an initial guess, and the vectors  $p_N^\ell := u_N^\ell - u_N^{\ell-1}$  represent the updates in each iteration step, which are pairwise orthogonal with respect to the inner product  $(\cdot, \cdot)_a$ . Note

that the CG method converges to the Galerkin solution  $u_N^h$  of (2.3) in at most  $N$  steps (in exact arithmetic), whence we observe the identity

$$u_N^h - u_N^n = u_N^N - u_N^n = \sum_{\ell=n+1}^N p_N^\ell.$$

Further, exploiting  $a$ -orthogonality, we obtain

$$\|u_N^h - u_N^n\|_a^2 = \sum_{\ell=n+1}^N \|p_N^\ell\|_a^2 \geq \sum_{\ell=n+1}^{n+d} \|p_N^\ell\|_a^2 =: \xi_n^d, \quad (2.7)$$

where the so-called *Hestenes-Stiefel (HS) estimate*  $\xi_n^d$  represents a lower bound on the iteration error in the energy norm (see [HS52]), and  $d \in [1 : N - n]$  is the so-called *delay parameter*. The CG method can naturally be interpreted as an energy minimization algorithm: indeed, in the  $\ell$ -th iteration, the energy is minimized over the affine linear set

$$\mathbb{V}_N^\ell := \{u_N^0 + v \mid v \in \text{span}\{p_N^1, \dots, p_N^\ell\}\}.$$

In the following lemma, we demonstrate that the Hestenes-Stiefel estimate can likewise be interpreted from an energy perspective.

**Lemma 2.** *The HS estimate (2.7) can be written equivalently as*

$$\xi_n^d = 2 (\mathbb{E}(u_N^n) - \mathbb{E}(u_N^{n+d})). \quad (2.8)$$

*Proof.* Employing Lemma 1, and making use of (2.7), we observe that

$$\begin{aligned} 2 (\mathbb{E}(u_N^n) - \mathbb{E}(u_N^{n+d})) &= \|u_N^h - u_N^n\|_a^2 - \|u_N^h - u_N^{n+d}\|_a^2 \\ &= \sum_{\ell=n+1}^N \|p_N^\ell\|_a^2 - \sum_{\ell=n+d+1}^N \|p_N^\ell\|_a^2 \\ &= \sum_{\ell=n+1}^{n+d} \|p_N^\ell\|_a^2 = \xi_n^d, \end{aligned}$$

which yields the claim.  $\square$

Summarizing, in order to minimize the energy over  $\mathbb{V}_N$ , we employ the CG algorithm as iterative solver which, in the  $\ell$ -th step, minimizes the energy over the affine linear set  $\mathbb{V}_N^\ell$  and whose iteration error can be estimated from below by the HS estimate (2.8).

**2.4. Stopping Criteria.** We will now present two stopping criteria that allow to obtain an appropriate final iterate  $u_N^*$  in the sequence  $\{u_N^n\}_n \subset \mathbb{V}_N$  generated by the CG algorithm.

**(a) Energy Tail-Off Stopping Criterion.** The first stopping criterion we introduce has been already employed in the work [AHW23]. Roughly speaking, the idea is to stop the iteration as soon as the sequence of energy values  $\{\mathbb{E}(u_N^n)\}_n \subset \mathbb{R}$  begins to level-off. To formalize this approach, let  $\Phi_N^n$  denote the accumulated energy decay up to the  $n$ -th iteration, i.e. for  $n \geq 1$ , let

$$\Phi_N^n := \mathbb{E}(u_N^0) - \mathbb{E}(u_N^n) \geq 0.$$

The iteration is stopped as soon as it holds

$$\mathbb{E}(u_N^{n-1}) - \mathbb{E}(u_N^n) < \alpha_E \Phi_N^n, \quad (2.9)$$

where  $\alpha_E \in (0, 1]$  is a prescribed control parameter. In this work, however, we slightly modify this criterion by dividing the right-hand side of (2.9) by the iteration number  $n$ , thereby turning the right-hand side into an averaged quantity over all iterations that is more restrictive; specifically, our new stopping criterion reads

$$\mathbb{E}(u_N^{n-1}) - \mathbb{E}(u_N^n) < \alpha_E \frac{\Phi_N^n}{n}, \quad (2.10)$$

with  $\alpha_E \in (0, 1]$  a control parameter as above.

**(b) Relative Energy Reduction Stopping Criterion.** The second stopping criterion we introduce is inspired by an approach proposed in [Ari04]. For any  $u_N^n \in \mathbb{V}_N$  (not necessarily resulting from the CG algorithm), they show that, whenever we have the bound

$$\|u_N^h - u_N^n\|_a \leq \gamma \|u_N^h\|_a, \quad (2.11)$$

for some parameter  $\gamma > 0$ , then it follows that

$$\|u - u_N^n\|_a \leq \gamma \|u\|_a + 2\|u - u_N^h\|_a, \quad (2.12)$$

where  $u \in \mathbb{V}$  and  $u_N^h \in \mathbb{V}_N$  are the full space solution and Galerkin solution, respectively, see [Ari04, Eq. (11)]. Hence, condition (2.11) may be regarded as an academic stopping criterion which, when satisfied, guarantees the inequality (2.12). Let us first discuss why this implication is of interest, before addressing the task of transforming (2.11) into a practical stopping criterion. To this end, suppose for a moment that a strategy for generating a sequence of finite-dimensional subspaces  $\{\mathbb{V}_N\}_{N \geq 0} \subset \mathbb{V}$  is available such that the associated Galerkin solutions  $u_N^h \in \mathbb{V}_N$  satisfy the asymptotic estimate

$$\|u - u_N^h\|_a = \mathcal{O}\left((\dim \mathbb{V}_N)^{-r}\right),$$

for a rate  $r \geq 1$ . The construction of such a sequence is discussed in Section 3. Then, on each subspace  $\mathbb{V}_N$ , choosing  $\gamma \propto (\dim \mathbb{V}_N)^{-r}$ , and iterating until (2.11) is satisfied for the final approximation  $u_N^*$ , the implication (2.12) yields

$$\|u - u_N^*\|_a = \mathcal{O}\left((\dim \mathbb{V}_N)^{-r}\right),$$

thus recovering the optimal convergence rate. With this motivation in place, we now turn to the task of transforming (2.11) into a practical stopping criterion by deriving computable estimates for both sides of the inequality.

A computable lower bound for the right-hand side of (2.11) can be obtained from Lemma 1. Indeed, from

$$\|u_N^h - u_N^n\|_a^2 - 2\mathbf{E}(u_N^n) = \|u_N^h\|_a^2,$$

we immediately deduce the estimate

$$-2\mathbf{E}(u_N^n) \leq \|u_N^h\|_a^2. \quad (2.13)$$

This inequality provides a practical and computable lower bound for the right-hand-side of (2.11), i.e. the energy norm of the Galerkin solution.

Deriving an a posteriori upper bound for the left-hand side of (2.11), i.e. the iteration error, is a far more challenging task. In fact, even when restricting ourselves to iterates generated by the CG algorithm, existing techniques typically depend on a priori spectral information of the system matrix, which entails non-negligible computational cost (see, e.g. [MT24]), and, more critically for our work, disregard the underlying energy structure of the problem. For these reasons, following the approach proposed in [Ari04], we rely on the HS estimate as an a posteriori estimator for the iteration error; although the HS estimate yields only a lower bound on the true iteration error, cf. (2.7) (whilst an upper bound would be required for reliability), this approach, which was also used in the original work [Ari04], has proven effective in our numerical experiments also. Further, in conjunction with Lemma 2, employing the HS estimate fits naturally into our energy-based framework.

Summarizing, we substitute the right-hand side of (2.11) with its lower bound (2.13), while the left-hand side of (2.11) is approximated by the HS estimate in its energy form (cf. Lemma 2). Further, as motivated above, for the  $\mathbb{P}_1$  finite element discretizations in the numerical experiments in Section 4, we set the parameter  $\gamma$  in (2.11) to  $\gamma^2 := \alpha_\gamma / \dim \mathbb{V}_N$  as we expect an optimal approximation rate of  $r = 1/2$ ; here,  $\alpha_\gamma \in (0, 1]$  is a control parameter. Finally, this yields the following computable a posteriori stopping criterion:

$$\mathbf{E}(u_N^n) - \mathbf{E}(u_N^{n+d}) \leq -\frac{\alpha_\gamma}{\dim \mathbb{V}_N} \mathbf{E}(u_N^n), \quad (2.14)$$

where  $d$  denotes the delay parameter used in the HS estimate. This means that the iteration is terminated at the  $n$ -th step once the relative energy reduction—measured between the current

iterate  $u_N^n$  and the delayed iterate  $u_N^{n+d}$ —falls below the threshold  $\gamma^2 = \alpha_\gamma / \dim \mathbb{V}_N$ . We emphasize that this stopping criterion is mathematically equivalent to the one proposed in [Ari04]. The key distinction is that we have reformulated it to emphasize its energy-based interpretation.

*Remark 2.* We conclude this Section with a few practical aspects.

- (a) In the article [Ari04] a strategy to adaptively choose the delay parameter on an ad hoc basis has been presented: Starting from an initial value  $d_{\text{init}} \geq 1$ , the delay parameter is updated by adding a fixed increment  $\Delta d \geq 1$  whenever the condition

$$\xi_{n+1}^d > \tau \xi_n^d \quad (2.15)$$

is met, where  $\tau > 1$  is a control parameter, i.e., we set  $d \leftarrow d + \Delta d$  as long as (2.15) holds true. The convergence test (2.14) is only applied once (2.15) is no longer satisfied. In this paper, we adopt this adaptive strategy in our numerical experiments in Section 4.

- (b) We have also tested a combined stopping criterion that consecutively applied the energy tail-off criterion (2.10) for global convergence and the relative energy reduction criterion (2.14) for local convergence (or the bound (2.16) for more general situations to be discussed below in Section 2.5). The resulting performance and convergence behavior were comparable to those obtained with the energy tail-off criterion alone, thereby providing no substantial improvements with regard to the qualitative or quantitative regime of the scheme. We therefore omit these results from the present discussion.
- (c) We note that the use of a preconditioner in the CG algorithm does not interfere with the stopping criteria presented in this Section. In particular, when employing the preconditioned conjugate gradient (PCG) method instead of CG, the stopping criteria can be applied exactly as described above without any modifications. Indeed, if  $\mathbf{x}_k, \hat{\mathbf{x}}_k$  denote the iterates of the CG and corresponding PCG algorithm, it can be verified that it holds

$$E(\mathbf{x}_k) = \hat{E}(\hat{\mathbf{x}}_k),$$

where  $E$  and  $\hat{E}$  denotes the energy of the system without and with preconditioning, respectively.

- (d) To reduce the sensitivity of the stopping criterion to local energy flattenings, one may evaluate criterion (2.10) in batches, that is, only for every  $n_{\text{batch}}$ -th iterate, where  $n_{\text{batch}} \geq 1$  is an integer-valued control parameter. This strategy has been adopted in Section 4.
- (e) In order to evaluate stopping criterion (2.14) for the  $n$ -th iterate, we need to compute the  $(n+d)$ -th iterate as well. As we focus on assessing the effectiveness of the stopping criterion from an academic perspective, the errors computed and shown in Section 4 always correspond to the  $n$ -th iterate, even though the  $(n+d)$ -th iterate is available. In a practical setting, however, one would naturally go along with the  $(n+d)$ -th iterate. Finally, we remark that the iteration counts shown in the corresponding plots do include the additional  $d$  steps required to evaluate the relative energy reduction stopping criterion (2.14).

**2.5. Application to more general minimization problems.** The iterative approximation of the Galerkin solution of the linear-quadratic energy functional (2.2) presented above, including the choice of iterative solver and stopping criteria, is primarily motivated by energy minimization principles. This observation naturally suggests extending this iterative strategy to more general energy minimization problems, where the underlying energy functional merely satisfies Assumption 1. In this setting, however, a few adjustments need to be made:

- (a) Firstly, the a posteriori stopping criterion (2.14) requires a slight modification. Indeed, for a monotonically decreasing sequence  $\{E(u_N^n)\}_n$ , note that the left-hand side of (2.14) is non-negative (cf. Lemma 1), and thus renders (2.14) ineffective whenever the energy minimum is positive (which, in contrast to the linear-quadratic case, is possible). A simple yet effective remedy is to employ absolute values, that is, to replace (2.14) by

$$|E(u_N^n) - E(u_N^{n+d})| \leq \frac{\alpha_\gamma}{\dim \mathbb{V}_N} |E(u_N^n)|. \quad (2.16)$$

This modification allows the stopping criterion to be interpreted in terms of the relative change in energy over  $d$  iterations and extends its applicability to more general energy minimization

problems. We emphasize that, in the linear-quadratic setting and sufficiently close to the minimizer, criterion (2.14) is *equivalent* to (2.16).

- (b) Secondly, the linear CG algorithm is no longer applicable when the weak formulation (1.3) is nonlinear. Instead, suitable alternatives are provided by nonlinear CG methods (for a comprehensive overview of nonlinear CG algorithms and their global convergence properties, we refer to [HZ06]). In corresponding numerical experiments in Section 4.1, we employ the existing implementation `scipy.optimize.fmin_cg` [Vir+20], which provides a nonlinear CG method based on the approach of Polak and Ribière [NW06]. However, the energy-based stopping criteria introduced above do, in principle, remain applicable without any modifications (cf. Section 4.1). For future reference we also introduce the *default* stopping criterion implemented in `scipy.optimize.fmin_cg`, which reads

$$\|\nabla E(u_N^n)\|_\infty \leq g_{\text{tol}}, \quad (2.17)$$

where  $\nabla E(u_N^n) \in \mathbb{R}^{\dim \mathbb{V}_N}$  denotes the gradient of  $E$  evaluated at the current iterate  $u_N^n$ , and  $g_{\text{tol}} \in [0, \infty)$  is a user-chosen control parameter. The default stopping criterion terminates the iteration at the  $n$ -th step, as soon as (2.17) is satisfied.

### 3. SPACE ENRICHMENT AND VARIATIONAL ADAPTIVITY

In this Section, given a (finite-dimensional) subspace  $\mathbb{V}_N \subset \mathbb{V}$  and a final iterate  $u_N^* \in \mathbb{V}_N$ , we present an energy-based, adaptive enrichment strategy to construct the subsequent (refined) subspace  $\mathbb{V}_{N+1} \subset \mathbb{V}_N$  aiming for the largest possible local energy reduction. We first present the algorithm in abstract form for a general Hilbert space  $\mathbb{V}$ , then give a concrete realization for  $\mathbb{P}_1$  finite element spaces on two-dimensional domains, and finally discuss computational aspects of the proposed framework. Throughout this Section, we assume that  $E : \mathbb{V} \rightarrow \mathbb{R}$  satisfies Assumption 1.

**3.1. Variational Adaptivity.** Given a subspace  $\mathbb{V}_N \subset \mathbb{V}$  and the final iterate  $u_N^* \in \mathbb{V}_N$ , let  $\xi = \{\xi_1, \dots, \xi_L\} \subset \mathbb{V}$  be a set of linearly independent elements such that the intersection  $\mathbb{V}_N \cap \xi = \emptyset$  is empty, and define the (low-dimensional) subspace  $\mathbb{Y} := \text{span}\{u_N^*, \xi_1, \dots, \xi_L\}$ . In this setting, we call  $\xi$  an *enrichment set* and  $\mathbb{Y}$  a (*local*) *enrichment space*; in the context of finite element discretizations, the space  $\mathbb{Y}$  is spanned by one global mode, namely the approximation  $u_N^*$ , and  $L$  additional degrees of freedom that act locally in the vicinity of a specific element in order to detect and resolve potential fine scale features in the full-space solution. By considering (1.3) with  $\mathbb{W} = \mathbb{Y}$ , we obtain the (low-dimensional) problem of finding  $u_{\mathbb{Y}}^h \in \mathbb{Y}$  such that it holds

$$E' [u_{\mathbb{Y}}^h] (y) = 0 \quad \forall y \in \mathbb{Y}. \quad (3.1)$$

We call  $u_{\mathbb{Y}}^h$  a *locally improved solution*, and note that it is equivalently characterized as the unique minimizer of  $E$  over  $\mathbb{Y}$ ; in particular, since  $u_N^* \in \mathbb{Y}$ , we immediately obtain the energy reduction property

$$E(u_{\mathbb{Y}}^h) \leq E(u_N^*).$$

We can thus define the non-negative *energy decay*

$$\Delta E(u_N^*, \xi) := E(u_N^*) - E(u_{\mathbb{Y}}^h) \geq 0. \quad (3.2)$$

The energy decay  $\Delta E(u_N^*, \xi)$  provides a computable a priori lower bound to the *potential energy reduction* resulting from enriching the space  $\mathbb{V}_N$  with the enrichment set  $\xi$ , i.e. by switching from  $\mathbb{V}_N$  to the augmented space  $\mathbb{V}_N \oplus \text{span } \xi$ .

The above considerations motivate the following strategy: Let  $\{\xi_\ell\}_{\ell=1, \dots, M}$  be a family of enrichment sets. For each of the enrichment sets we can compute the corresponding energy decay (3.2). Then, choose an index subset  $\mathcal{I} \subset \{1, \dots, M\}$  of minimal cardinality that fulfills the classical Dörfler marking criterion [Dör96]; in the language of energy decays, this criterion reads

$$\sum_{\ell \in \mathcal{I}} \Delta E(u_N^*, \xi_\ell) \geq \theta \sum_{\ell=1}^M \Delta E(u_N^*, \xi_\ell), \quad (3.3)$$

where  $\theta \in (0, 1)$  is the *Dörfler parameter*. Finally, define

$$\mathbb{V}_{N+1} := \mathbb{V}_N \oplus \text{span} \bigcup_{\ell \in \mathcal{I}} \boldsymbol{\xi}_\ell, \quad (3.4)$$

and apply the natural embedding

$$u_{N+1}^0 := u_N^* \hookrightarrow \mathbb{V}_{N+1},$$

to define a starting point for approximating the minimizer  $u_{N+1}^h$  of  $\mathbb{E}$  within the subsequent subspace  $\mathbb{V}_{N+1}$ . The resulting process that iteratively generates a nested sequence of subspaces is outlined in Algorithm 1 and is referred to as *variational adaptivity*. The application of this algorithm within a finite element context is discussed in Section 3.2.

*Remark 3.* In the linear-quadratic case (cf. Section 2.1), problem (3.1) reduces to an  $(L_j + 1) \times (L_j + 1)$  linear system, where  $L_j$  is the number of elements in  $\boldsymbol{\xi}_j$ . Solving this system exactly is computationally inexpensive, as  $L_j$  is usually small. More generally, however, if the underlying energy only satisfies Assumption 1, it is typically impossible to solve the local problem (3.1) in closed form as it may be nonlinear. In such cases, one can accurately approximate the exact solution by applying an appropriate nonlinear solver, e.g., a Newton-type scheme, that results in a sequence of  $(L_j + 1) \times (L_j + 1)$  linear systems.

---

**Algorithm 1** Variational adaptivity

---

1. Prescribe the Dörfler parameter  $\theta \in (0, 1)$ .
  2. Input a finite-dimensional subspace  $\mathbb{V}_N \subset \mathbb{V}$ , a suitable approximation  $u_N^* \in \mathbb{V}_N$ , and a family of enrichment sets  $\{\boldsymbol{\xi}_\ell\}_{\ell=1, \dots, M}$  not contained in  $\mathbb{V}_N$ .
  3. **for**  $\ell = 1, \dots, M$  **do**
  4.   SOLVE the (low-dimensional) problem (3.1) for  $u_{\mathbb{V}}^h \in \mathbb{V}$ .
  5.   Compute the corresponding energy decay (3.2).
  6. **end for**
  7. CHOOSE an index subset  $\mathcal{I} \subset \{1, \dots, M\}$  based on the Dörfler marking criterion (3.3).
  8. ENRICH the space  $\mathbb{V}_N$  according to (3.4), thereby yielding the subsequent linear subspace  $\mathbb{V}_{N+1} \supset \mathbb{V}_N$ .
- 

**3.2. Edge-based Variational Adaptivity.** Let  $\Omega \subset \mathbb{R}^2$  be an open and bounded polygonal domain and  $H_0^1(\Omega)$  the first-order Sobolev space with zero trace on  $\partial\Omega$ . Then, in this subsection, we illustrate how the abstract framework introduced in Section 3.1 can be used to adaptively refine a two-dimensional simplicial mesh underlying a  $\mathbb{P}_1$  finite element discretization of  $H_0^1(\Omega)$ . Specifically, we discuss how edge bisections can be interpreted as local space enrichments and the resulting augmentation (3.4) as mesh refinement. In combination with the iterative solver developed in Section 2, this enables the construction of an adaptive and fully iterative algorithm for minimizing energy functionals over  $H_0^1(\Omega)$  using  $\mathbb{P}_1$  finite element discretizations in two spatial dimensions, to be employed in numerical experiments in Section 4. Note that this implementation of variational adaptivity contrasts earlier works [AHW23; HSW21; HW25], which have employed a similar approach, especially in the sense that they have used *local red refinement* of individual elements to compute the energy reduction indicators, whereas we rely on more localized edge bisections.

**3.2.1. The  $\mathbb{P}_1$  Finite Element Space.** For  $N \geq 0$ , we consider a triangulation  $\mathcal{T}_N$  consisting of disjoint open triangles  $\{T\}_{T \in \mathcal{T}_N}$  that form a regular and shape-regular mesh partition of the domain  $\Omega$ . The corresponding  $\mathbb{P}_1$  conforming finite element space is then given by

$$\mathbb{P}_1(\mathcal{T}_N) := \left\{ \varphi \in H_0^1(\Omega) \mid \forall T \in \mathcal{T}_N : \varphi|_T \in \mathbb{P}_1(T) \right\}.$$

Further, let  $\mathcal{E}_N$  denote the set of all edges in the triangulation  $\mathcal{T}_N$ , and  $\mathcal{V}_N$  the set of all of its vertices. For future reference, we define  $\mathcal{E}_N^I \subset \mathcal{E}_N$  and  $\mathcal{V}_N^I \subset \mathcal{V}_N$  to be the set of all interior edges

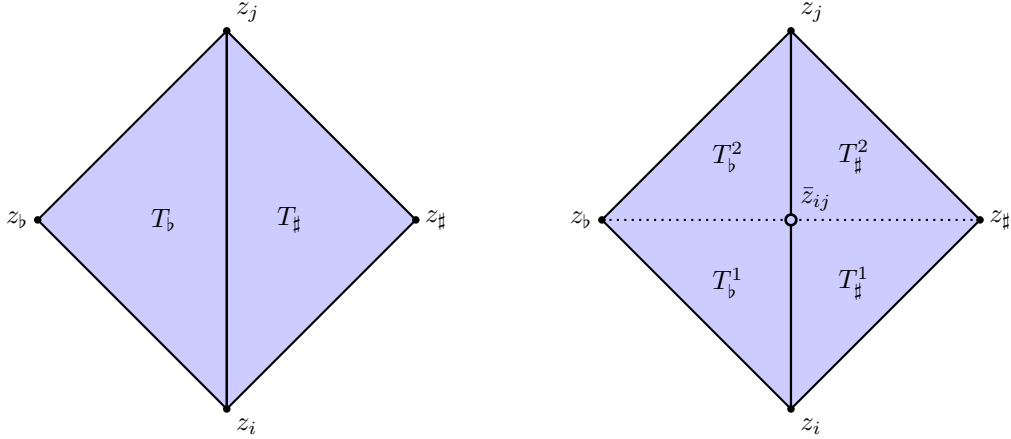


FIGURE 1. Local patches associated to an interior edge  $E = (z_i, z_j)$ . Left: local patch  $\omega_E$  before the local refinement. Right: local modified patch  $\tilde{\omega}_E$  obtained by bisection of the edge  $E$  and removing the hanging node  $\tilde{z}_{ij}$  by connecting it to both vertices  $z_#$  and  $z_b$ .

and of all interior vertices, respectively. In this context, we define  $d_N := \dim \mathbb{V}_N$  to be the number of degrees of freedom in the discrete space  $\mathbb{P}_1(\mathcal{T}_N)$ , i.e. the number of interior vertices  $d_N = \#\mathcal{V}_N^I$ . As a basis of  $\mathbb{P}_1(\mathcal{T}_N)$  we introduce the usual Lagrange hat basis functions  $\{\phi_i\}_{i=1, \dots, d_N} \subset \mathbb{P}_1(\mathcal{T}_N)$ , uniquely defined by  $\phi_i(z_j) = \delta_{ij}$ ,  $z_j \in \mathcal{V}_N^I$ , where  $\delta_{ij}$  denotes the Kronecker delta. Then, any discrete approximation  $u_N \in \mathbb{P}_1(\mathcal{T}_N)$  can be written as

$$u_N = \sum_{j=1}^{d_N} U_N^j \phi_j,$$

where  $U_N^j \in \mathbb{R}$ ,  $1 \leq j \leq d_N$ , cf. (2.5).

*Remark 4.* Throughout this work, we restrict ourselves to piecewise linear finite elements. This choice allows us to present the main concepts of our approach in the least technical setting. The variational adaptivity framework, however, is not limited to linear elements. In fact, the ideas can be generalized to higher-order finite elements and even to  $hp$ -methods (see, e.g. [BSW25]).

**3.2.2. Edge-Based Space Enrichments.** The following procedure is a concrete, edge-based realization of *variational adaptivity*, translating edge bisections into local space enrichments. For each interior edge  $E \in \mathcal{E}_N^I$ , we define a corresponding enrichment set  $\xi_E$  (here, a singleton) that is constructed via bisection of the edge  $E$  as follows: Let  $E = \text{conv}\{z_i, z_j\} \in \mathcal{E}_N^I$  be any interior edge connecting two vertices  $z_i, z_j \in \mathcal{V}_N$ , where  $\text{conv}\{\cdot\}$  denotes (the open interior of) the convex hull. Then, consider the *local patch*  $\omega_E$  comprising the two elements  $T_#, T_b \in \mathcal{T}_N$  that share the edge  $E$ , i.e.  $\omega_E := \{T_#, T_b\}$ . Further, let  $z_#, z_b \in \mathcal{V}_N$  denote the remaining vertices of the local patch on either side of  $E$ ; a sketch of this configuration is shown in Figure 1. Define  $\tilde{z}_{ij} \in E$  as the midpoint of  $E$ , i.e.  $\tilde{z}_{ij} := 1/2(z_i + z_j)$ , and consider the open triangles

$$\begin{aligned} T_#^1 &:= \text{conv}\{z_i, \tilde{z}_{ij}, z_#\}, & T_#^2 &:= \text{conv}\{z_j, \tilde{z}_{ij}, z_#\}, \\ T_b^1 &:= \text{conv}\{z_i, \tilde{z}_{ij}, z_b\}, & T_b^2 &:= \text{conv}\{z_j, \tilde{z}_{ij}, z_b\}, \end{aligned}$$

which are the triangles obtained by splitting both  $T_#$  and  $T_b$  through connections from  $\tilde{z}_{ij}$  to  $z_#$  and  $z_b$ , respectively. We define the modified (refined) patch as  $\tilde{\omega}_E := \{T_#^1, T_#^2, T_b^1, T_b^2\}$ . Next, we introduce a hat function  $\phi_E \in H_0^1(\Omega)$  associated to the new vertex  $\tilde{z}_{ij}$  that is uniquely defined by requiring  $\phi_E|_\tau \in \mathbb{P}_1(\tau)$  for all elements  $\tau \in \tilde{\omega}_E \cup (\mathcal{T}_N \setminus \omega_E)$ , and

$$\forall z \in \mathcal{V}_N \cup \{\tilde{z}_{ij}\}: \quad \phi_E(z) = \begin{cases} 1 & \text{if } z = \tilde{z}_{ij}, \\ 0 & \text{otherwise.} \end{cases}$$

We then define the enrichment set associated with edge  $E$  as the singleton  $\boldsymbol{\xi}_E := \{\phi_E\}$ . Following this procedure for all interior edges yields a family of enrichment sets  $\{\boldsymbol{\xi}_E\}_{E \in \mathcal{E}^I}$ . Then, we proceed according to Algorithm 1, i.e. we compute the non-negative energy decays  $\Delta \mathbf{E}(u_N^*, \boldsymbol{\xi}_E)$  from (3.2) and select a suitable subset that fulfills the Dörfler marking criterion (3.3). The corresponding edges we refer to as *marked edges*. The proposed edge-based variational adaptivity procedure is summarized in Algorithm 2.

**3.3. Computational Aspects.** The practical application of the abstract framework above, in particular regarding the solution of (3.1) and the space enrichment (3.4), will be discussed in the specific context of  $\mathbb{P}_1$  finite element discretizations in the following subsections.

**3.3.1. Mesh Refinement.** When working with  $\mathbb{P}_1$  finite element spaces, the abstract space enrichment procedure in (3.4) needs some fine adjustments. To see why, recall that, for any  $h$ -FEM, additional degrees of freedom are introduced through mesh refinement. Such refinements, however, must be performed carefully in order to maintain mesh regularity and to prevent degeneration. Edge-based Variational Adaptivity, as outlined in Section 3.2, leaves us with a subset of marked edges. We make sure to both bisect all marked edges and to preserve the mesh quality by inputting the mesh and its marked edges into the well-known newest-vertex bisection (NVB) algorithm as described in [FPW11, Section 5]. This refinement procedure then replaces (3.4), i.e. the refined mesh defines the subsequent  $\mathbb{P}_1$  finite element space.

---

**Algorithm 2** Edge-based variational adaptivity

---

1. Prescribe the Dörfler parameter  $\theta \in (0, 1)$ .
  2. Input a finite element mesh  $\mathcal{T}_N$  and a finite element function  $u_N^* \in \mathbb{P}_1(\mathcal{T}_N)$ .
  3. **for**  $E \in \mathcal{E}_N^I$  **do**
  4. SOLVE (3.1) with  $\mathbb{Y} = \text{span}(\{u_N^*\} \cup \boldsymbol{\xi}_E)$  for  $u_{\mathbb{Y}}^h \in \mathbb{Y}$ .
  5. Compute the corresponding energy decay  $\Delta \mathbf{E}(u_N^*, \boldsymbol{\xi}_E)$ , cf. (3.2).
  6. **end for**
  7. MARK a subset of the interior edges  $\mathcal{E}_N^I$  of minimal cardinality fulfilling the Dörfler marking criterion (3.3) for refinement.
  8. REFINED the mesh  $\mathcal{T}_N$  based on the marked edges using newest-vertex bisection (NVB) as described in [FPW11, Section 5] to obtain the refined mesh  $\mathcal{T}_{N+1}$  and build the corresponding finite element space  $\mathbb{P}_1(\mathcal{T}_{N+1}) \supset \mathbb{P}_1(\mathcal{T}_N)$ .
- 

**3.3.2. Computation of energy decay.** If the energy  $\mathbf{E} : \mathbb{V} \rightarrow \mathbb{R}$  merely satisfies Assumption 1, we generally need to resort to a two-fold approximation of the local energy decay (3.2). First, the local minimization problem (3.1) cannot typically be solved exactly, cf. Remark 3. Instead, we compute an approximation  $\tilde{u}_{\mathbb{Y}} \approx u_{\mathbb{Y}}^h$  as follows. Assuming that  $\mathbf{E}$  is twice Gâteaux differentiable, we set  $\delta := \tilde{u}_{\mathbb{Y}} - u_N^*$  and consider the first-order approximation of (3.1), i.e.

$$\mathbf{E}''[u_N^*](\delta, y) = -\mathbf{E}'[u_N^*](y) \quad \forall y \in \mathbb{Y}, \quad (3.5)$$

whose solution can be obtained by solving the corresponding (low-dimensional) linear system. Second, given the solution  $\tilde{u}_{\mathbb{Y}}$  of (3.5), the corresponding energy decay would be obtained by evaluating (3.2) with  $u_{\mathbb{Y}}^h$  replaced by  $\tilde{u}_{\mathbb{Y}}$ . However, performing this evaluation for every enrichment set can become prohibitively expensive (in the context of finite elements this becomes obvious due to the global integrals involved in the energy). Hence, we employ a computationally cheaper approximate predictor. To this end, applying the main theorem of calculus, we note that it holds

$$\mathbf{E}(\tilde{u}_{\mathbb{Y}}) - \mathbf{E}(u_N^*) = \mathbf{E}'[u_N^*](\delta) + \int_0^1 (\mathbf{E}'[u_N^* + s\delta](\delta) - \mathbf{E}'[u_N^*](\delta)) ds. \quad (3.6)$$

We use the first term on the right-hand side as a first-order approximation for the negative energy decay, that is

$$\mathbf{E}(\tilde{u}_{\mathbb{Y}}) - \mathbf{E}(u_N^*) \approx \mathbf{E}'[u_N^*](\delta). \quad (3.7)$$

By (3.5) and the strong convexity of  $\mathbf{E}$ , we observe that this predictor is guaranteed to be non-positive. Incidentally, applying a second-order Taylor expansion, viz.

$$\mathbf{E}'[u_N^* + s\delta](\delta) = \mathbf{E}'[u_N^*](\delta) + s\mathbf{E}''[u_N^*](\delta, \delta) + \mathcal{O}(\delta^3),$$

and exploiting (3.5) with  $y = \delta$ , the integral in (3.6) can be expressed by

$$\int_0^1 (\mathbf{E}'[u_N^* + s\delta](\delta) - \mathbf{E}'[u_N^*](\delta)) \, ds = \frac{1}{2}\mathbf{E}''[u_N^*](\delta, \delta) + \mathcal{O}(\delta^3) = -\frac{1}{2}\mathbf{E}'[u_N^*](\delta) + \mathcal{O}(\delta^3).$$

Thus, we infer that

$$\mathbf{E}(\tilde{u}_{\mathbb{Y}}) - \mathbf{E}(u_N^*) = \frac{1}{2}\mathbf{E}'[u_N^*](\delta) + \mathcal{O}(\delta^3). \quad (3.8)$$

Consequently, in the Dörfler marking (3.3) (where constant factors cancel), using the first-order predictor (3.7) is equivalent to neglecting the  $\mathcal{O}(\delta^3)$  terms in the above energy-decay approximation (3.8). In summary, the approximation of the local energy decay is indeed two-fold: We approximate the exact minimizer  $\tilde{u}_{\mathbb{Y}} \approx u_{\mathbb{Y}}^h$  using (3.5), and the energy decay corresponding to  $\tilde{u}_{\mathbb{Y}}$  using (3.7) (or equivalently (3.8)).

We continue by briefly discussing how the local energy decays can be computed in practice. In the special case where the energy functional  $\mathbf{E} : \mathbb{V} \rightarrow \mathbb{R}$  is linear-quadratic (cf. Section 2.1), we may compute both the locally improved solution and its corresponding energy decay exactly. To see this, consider, for example, edge-based variational adaptivity (cf. Section 3.2). Then, problem (3.1) is equivalent to the  $2 \times 2$  linear system

$$\begin{pmatrix} a(u_N^*, u_N^*) & a(u_N^*, \phi_E) \\ a(\phi_E, u_N^*) & a(\phi_E, \phi_E) \end{pmatrix} \begin{pmatrix} \alpha \\ \beta \end{pmatrix} = \begin{pmatrix} \ell(u_N^*) \\ \ell(\phi_E) \end{pmatrix}, \quad (3.9)$$

such that  $u_{\mathbb{Y}}^h = \alpha u_N^* + \beta \phi_E$ , where  $\alpha, \beta \in \mathbb{R}$  solve (3.9). Note that the (global) terms  $a(u_N^*, u_N^*)$  and  $\ell(u_N^*)$  are both independent of individual edges  $E \in \mathcal{E}_N^I$ , and therefore, need to be computed once only. Moreover, owing to the highly localized support of the basis function  $\phi_E$ , the remaining entries of both the left-hand side matrix and the right-hand side vector in (3.9), which depend on  $E$ , reduce to local integrals. In addition, we note that the  $2 \times 2$  linear system (3.9) admits a closed-form solution. In this setting, the energy decay (3.2) reduces to

$$\Delta \mathbf{E}(u_N^*, \xi_E) = \mathbf{E}(u_N^*) - \mathbf{E}(u_{\mathbb{Y}}^h) = \frac{(1 - \alpha)^2}{2} a(u_N^*, u_N^*) - \beta(1 - \alpha) a(u_N^*, \phi_E) + \frac{\beta^2}{2} a(\phi_E, \phi_E). \quad (3.10)$$

We observe that the computation of the energy decay per edge (3.10) is highly parallelizable, and essentially involves only two global evaluations for the entire mesh, i.e. the quantities  $a(u_N^*, u_N^*)$  and  $\ell(u_N^*)$ .

For a general energy functional  $\mathbf{E} : \mathbb{V} \rightarrow \mathbb{R}$  satisfying Assumption 1, problem (3.5) inherits the same structure as (3.9), where the size of the system is determined by the number of elements in the enrichment set at hand.

*Remark 5.* For a linear-quadratic energy functional  $\mathbf{E}$ , the approximations (3.5) and (3.7) yield an equivalent marking strategy as performing the exact computations. To see this, consider the following. First, the linearized problem (3.5) indeed reduces to (3.9) and hence, yields the exact minimizer  $\tilde{u}_{\mathbb{Y}} = u_{\mathbb{Y}}^h \in \mathbb{Y}$ . Second, as  $\mathcal{O}(\delta^3)$  terms vanish, expression (3.8) tells us that, up to a factor  $1/2$ , the first order predictor corresponds to the exact energy decay. Hence, in the Dörfler marking strategy (3.3), the resulting set of marked edges agree for the approximate and exact computations.

*Remark 6.* At first glance, our approach might appear reminiscent of the classical Zienkiewicz-Zhu (ZZ) error estimator (see, e.g. [AO00, Chapter 4.6.1]). We emphasize, however, that the ZZ estimator aims at an a posteriori bound for the error, whilst our method is based on computing local *energy reduction indicators*. Furthermore, the ZZ estimator is recovery-based, i.e., it estimates the local error by suitably reconstructing the gradient of the current approximation, which, in contrast to the variational adaptivity concept, is computed using local information only; indeed, crucially in our framework, a potentially improved approximation of the given solution is computed using

a *global mode* and a local (low-dimensional) enrichment of the approximation space at any edge  $E \in \mathcal{E}_N^I$ , cf. (3.5).

**3.4. Fully iterative solver.** All the machinery needed to derive a fully iterative adaptive solver for problem (1.2) with  $\mathbb{V} = \mathbb{H}_0^1(\Omega)$  is now in place and outlined in Algorithm 3. Roughly speaking, our approach consists of two intertwined strategies:

1. On a given finite dimensional subspace  $\mathbb{P}_1(\mathcal{T}_N) \subset \mathbb{H}_0^1(\Omega)$ , we perform (nonlinear) CG iterations until one of the stopping criteria described in Section 2.4 is met, thereby yielding a final iterate  $u_N^* \in \mathbb{P}_1(\mathcal{T}_N)$  (Line 4 in Algorithm 3).
2. We use the final iterate  $u_N^* \in \mathbb{P}_1(\mathcal{T}_N)$  to compute local energy reduction indicators within the framework of edge-based variational adaptivity as described in Section 3.2. Combined with the Dörfler marking strategy, these indicators determine a subset of interior edges to be refined. To guarantee that the refinement process preserves mesh shape regularity and avoids degenerating elements, we employ NVB as outlined in [FPW11, Section 5] to refine the mesh and to finally construct the subsequent finite element space  $\mathbb{P}_1(\mathcal{T}_{N+1})$  (Line 5 in Algorithm 3).

After these two steps have been completed, an initial guess  $u_{N+1}^0 \in \mathbb{P}_1(\mathcal{T}_{N+1})$  is constructed by linearly interpolating the final iterate  $u_N^*$  onto the refined mesh (Line 6 in Algorithm 3). Finally, the procedure is restarted and repeated until a specified maximum number of degrees of freedom is reached or, alternatively, until the relative energy decay of the sequence of the final iterates on each space, i.e.  $\{E(u_N^*)\}_N$ , falls below a predefined threshold.

---

**Algorithm 3** Fully iterative edge-based variational adaptivity  $\mathbb{P}_1$ -FEM

---

1. Prescribe the Dörfler parameter  $\theta \in (0, 1)$ , a maximum number of degrees of freedom  $N_{\max}$ , choose one of the stopping criteria described in Section 2.4, and fix the control parameter set needed for the chosen stopping criterion.
  2. Input an initial mesh  $\mathcal{T}_N$ , and an initial guess  $u_N^0 \in \mathbb{P}_1(\mathcal{T}_N)$ .
  3. **while**  $\dim \mathbb{P}_1(\mathcal{T}_N) \leq N_{\max}$  **do**
  4. Initialize (nonlinear) CG iterations with  $u_N^0$  and stop the iteration at  $u_N^*$  as soon as the chosen stopping criterion is met.
  5. Based on  $u_N^*$  and the current mesh  $\mathcal{T}_N$ , perform the edge-based variational adaptivity procedure as indicated in Algorithm 2 to obtain a refined mesh  $\mathcal{T}_{N+1}$  and the corresponding enriched finite element space  $\mathbb{P}_1(\mathcal{T}_{N+1})$ .
  6. Define  $u_{N+1}^0 := u_N^*$ , set  $N \leftarrow N + 1$ , and reset all control parameters from the chosen stopping criterion that might have been changed during the CG iterations.
  7. **end while**
- 

#### 4. NUMERICAL EXPERIMENTS

In this Section, we perform a series of numerical tests for Algorithm 3. Namely, on an open and bounded polygonal domain  $\Omega \subset \mathbb{R}^2$ , which will be either chosen to be the *L-shaped domain*  $\Omega_L := (-1, 1)^2 \setminus ([0, 1] \times [-1, 0])$ , or the *square domain*  $\Omega_S := (0, 1)^2$ , we consider the numerical solution of the semilinear elliptic diffusion-reaction boundary value problem (BVP):

$$\begin{aligned} -\nabla \cdot (\mathbf{A}(\mathbf{x}) \nabla u(\mathbf{x})) + \phi(u(\mathbf{x})) &= f(\mathbf{x}), & \mathbf{x} \in \Omega, \\ u(\mathbf{x}) &= 0, & \mathbf{x} \in \partial\Omega, \end{aligned} \tag{4.1}$$

where  $\phi \in C^0(\mathbb{R})$  is non-decreasing,  $f \in L^2(\Omega)$ , and  $\mathbf{A} : \Omega \rightarrow \mathbb{R}^{2 \times 2}$  is a piecewise constant symmetric diffusion matrix that is uniformly positive definite, i.e. there exists a constant  $C > 0$  such that

$$\forall \mathbf{x} \in \Omega : \inf_{\substack{\boldsymbol{\xi} \in \mathbb{R}^2 \\ \boldsymbol{\xi} \neq \mathbf{0}}} \frac{\boldsymbol{\xi}^\top \mathbf{A}(\mathbf{x}) \boldsymbol{\xi}}{\boldsymbol{\xi}^\top \boldsymbol{\xi}} \geq C.$$

Then, the BVP (4.1) admits a unique solution  $u \in \mathbb{H}_0^1(\Omega)$  [Glo84, chapter 4]; in our numerical tests below, the data will be specified individually for each experiment.

We define the energy functional  $\mathbf{E} : H_0^1(\Omega) \rightarrow \mathbb{R}$  corresponding to (4.1) as

$$\mathbf{E}(v) := \frac{1}{2} \int_{\Omega} \mathbf{A}(\mathbf{x}) \nabla v(\mathbf{x}) \cdot \nabla v(\mathbf{x}) \, d\mathbf{x} + \int_{\Omega} \Phi(v(\mathbf{x})) \, d\mathbf{x} - \int_{\Omega} f(\mathbf{x})v(\mathbf{x}) \, d\mathbf{x}, \quad (4.2)$$

with  $\Phi' = \phi$ . Indeed,  $\mathbf{E}$  satisfies Assumption 1 and hence, there exists a unique minimizer  $u \in H_0^1(\Omega)$  of  $\mathbf{E}$  that is also the weak solution of (4.1), cf. Section 1. Furthermore, the gradient term in the energy induces an energy norm on  $H_0^1(\Omega)$ , viz.

$$\|u\|_a^2 := \int_{\Omega} \mathbf{A}(\mathbf{x}) \nabla u(\mathbf{x}) \cdot \nabla u(\mathbf{x}) \, d\mathbf{x}.$$

In order to ensure that the respective iterative solver employed is able to sufficiently progress before convergence towards the (exact) Galerkin solution is assessed, a small number of iterations, denoted by  $n_{\min}$ , is enforced on each subspace before evaluating the respective stopping criterion. In particular, when using the energy tail-off stopping criterion (2.10), the condition is reformulated as

$$\mathbf{E}(u_N^n) - \mathbf{E}(u_N^{n-1}) < \alpha_E \frac{\mathbf{E}(u_N^{n_{\min}}) - \mathbf{E}(u_N^n)}{n - n_{\min}}, \quad \text{once } n > n_{\min}. \quad (4.3)$$

Moreover, owing to the adaptive adjustment of the delay parameter  $d$ , see Remark 2 (a), we emphasize that its value may vary during the (nonlinear) CG iterations on a given mesh, however, is always reset to  $d_{\text{init}}$  after each mesh refinement, cf. Line 6 in Algorithm 3.

In the performance plots, which we display for each numerical test, the stopping criteria are denoted as follows: criterion (2.10) is referred to as *energy tail-off*, criterion (2.16) as *relative energy reduction*, and criterion (2.17) as *default*. In addition, the following control parameters are available to be chosen in each of the experiments:

- The Dörfler parameter  $\theta \in (0, 1)$  in (3.3) (set to  $\theta = 0.5$  in *all* experiments),
- the control parameter  $\alpha_E$  of the energy tail-off stopping criterion (4.3),
- the control parameter  $\alpha_\gamma$  of the relative energy decay stopping criterion (2.16),
- the initial delay  $d_{\text{init}} \geq 1$ , fixed delay increment  $\Delta d \geq 1$ , and control parameter  $\tau > 1$  for the adaptive delay parameter corresponding to (2.15) and (2.16),
- the minimum number of iterations  $n_{\min}$  performed on each mesh before any stopping criterion is evaluated,
- the batch size  $n_{\text{batch}} \geq 1$  specifying the number of iterations between consecutive evaluations of the respective stopping criterion,
- and the threshold  $g_{\text{tol}}$  of the default stopping criterion (2.17) (necessary only in the nonlinear experiments and set to  $g_{\text{tol}} = 10^{-8}$  in *all* the nonlinear experiments).

As a visual reference, in all of our convergence plots, we will display a dashed line with slope  $-1/2$  (or  $-1$ ) corresponding to the optimal convergence rate for the energy norm (or its square) with respect to the number of degrees of freedom in  $\mathbb{P}_1$ -FEM for second order elliptic problems in two dimensions.

Any use of an existing implementation in `scipy` [Vir+20] is based on version 1.13.1, and all calculations were performed on the HPC cluster UBELIX ([id.unibe.ch/hpc](http://id.unibe.ch/hpc)) at the University of Bern.

The remainder of this Section is divided into two main parts: in Section 4.1, we consider the case where the reaction  $\phi$  is nonlinear, whereas in Section 4.2 we focus on the case where  $\phi$  is linear.

**4.1. Nonlinear Experiments.** In this Section, we assess Algorithm 3 for the numerical minimization of the energy functional (4.2) in the case where  $\phi$  is nonlinear. As motivated in Section 2.5, the iterative solver employed on each subspace is chosen to be the Polak–Ribière type nonlinear CG method implemented in `scipy.optimize.fmin_cg`. In all experiments below, the computational domain is the L-shaped domain  $\Omega_L$ . The specific choices of the control parameters are presented in the respective experiments below. We consider four distinct boundary value problems, where, for each problem, we report results for both stopping criteria presented in Section 2.4 and, as a reference, for the default stopping criterion (2.17) implemented in `scipy.optimize.fmin_cg`.

*Computational Setup.* Recall from Section 3.3.2 that we assume  $\mathbf{E}$  to be twice Gâteaux differentiable such that the locally improved solution may be obtained by solving (3.5). Here, this translates into assuming the nonlinearity  $\phi$  to be continuously differentiable, i.e.  $\phi \in C^1(\mathbb{R})$ .

Note that for Experiments 1–3, the exact full-space solution  $u \in H_0^1(\Omega)$  is unknown. Consequently, in the plots displaying the energy difference between the final iterates and the energy of the full-space solution, the latter is approximated by the energy of a reference solution  $\tilde{u} \approx u$  computed on a graded mesh towards the origin in the L-shaped domain  $\Omega_L$ , where all of our test problems are expected to exhibit a typical elliptic corner singularity; the strategy employed to create the graded mesh and the solver used to obtain the reference solutions thereon are both outlined in [SW25]<sup>1</sup>. In contrast, Experiment 4 is based on a manufactured solution, and therefore, we are able to compute the energy-norm error between the exact full-space solution and the final iterates.

All experiments below were initialized as follows. First, the mesh of the underlying domain was uniformly refined until a sufficiently large number of degrees of freedom was obtained. Second, the nonlinear CG method `scipy.optimize.fmin_cg` was applied using the default stopping criterion (2.17) with its default parameter settings. Finally, the mesh was refined using edge-based variational adaptivity as described in Algorithm 2, and the subsequent experiment was initialized on this refined mesh, with the initial guess given by the final iterate, embedded into the new space. All numerical integrations have been carried out using a quadrature rule with degree of exactness 6.

Finally, we point out that, in all experiments below, we employ the default stopping criterion with  $g_{\text{tol}} = 10^{-8}$ , which is three orders of magnitude smaller than the value suggested by the default settings. Consequently, the corresponding values in the plots below may be regarded as good approximations of the discretization energy (norm) error and serve as an indicator of the effectiveness of the proposed refinement strategy.

*Experiment 1.* In this experiment, we consider the BVP (4.1) with the constant diffusion matrix  $\mathbf{A} := \text{Id}$ , the nonlinearity  $\phi(u) := u^3$  (corresponding to the potential  $\Phi(u) = \frac{1}{4}u^4$ ), and the constant right-hand side function  $f := 1$ . The convergence plot in Figure 2 displays results for Algorithm 3 with the following choices of the control parameters for the corresponding stopping criteria. Relative energy reduction:  $\alpha_\gamma = 0.1$ ,  $n_{\text{min}} = 10$ ,  $\tau = 1.01$ ,  $d_{\text{init}} = 10$ ,  $\Delta d = 5$ . Energy tail-off:  $\alpha_E = 0.01$ ,  $n_{\text{min}} = 10$ ,  $n_{\text{batch}} = 5$ . Default:  $n_{\text{min}} = 10$ ,  $g_{\text{tol}} = 10^{-8}$ .

In Figure 2, we observe that both the relative energy reduction stopping criterion (2.16) and the energy tail-off stopping criterion (2.10) exhibit optimal convergence behavior, although the corresponding data points are located about half an order of magnitude above those obtained with the default stopping criterion (2.17). Finally, we observe that, compared to the default stopping criterion, our new energy-based criteria require considerably fewer space enrichment steps.

*Experiment 2.* In this experiment, we consider the BVP (4.1) with the constant diffusion matrix  $\mathbf{A} := \text{Id}$ , the nonlinearity  $\phi(u) := |u|u$  (corresponding to  $\Phi(u) = \frac{1}{3}|u|^3$ ), and the constant right-hand side function  $f := 1$ . The convergence plot in Figure 2 displays results for Algorithm 3 with the following choices of the control parameters for the corresponding stopping criteria. Relative energy reduction:  $\alpha_\gamma = 0.1$ ,  $n_{\text{min}} = 10$ ,  $\tau = 1.01$ ,  $d_{\text{init}} = 10$ ,  $\Delta d = 5$ . Energy tail-off:  $\alpha_E = 0.01$ ,  $n_{\text{min}} = 10$ ,  $n_{\text{batch}} = 5$ . Default:  $n_{\text{min}} = 10$ ,  $g_{\text{tol}} = 10^{-8}$ .

In Figure 3, we observe that the energy tail-off stopping criterion (2.10) performs considerably better than the relative energy reduction stopping criterion (2.16). The slope corresponding to the latter even appears to slightly level off asymptotically. Nevertheless, the results obtained with both the default stopping criterion and the energy tail-off stopping criterion closely follow the dashed line, indicating optimal convergence behavior in both cases. We therefore conclude that the adaptive edge-based refinement strategy is capable of resolving the corner singularity at the origin not only when using the final iterate produced by the default stopping criterion, but also when using the final iterate obtained with the energy tail-off stopping criterion.

---

<sup>1</sup>The authors gratefully acknowledge Florian Spicher for providing the corresponding code.

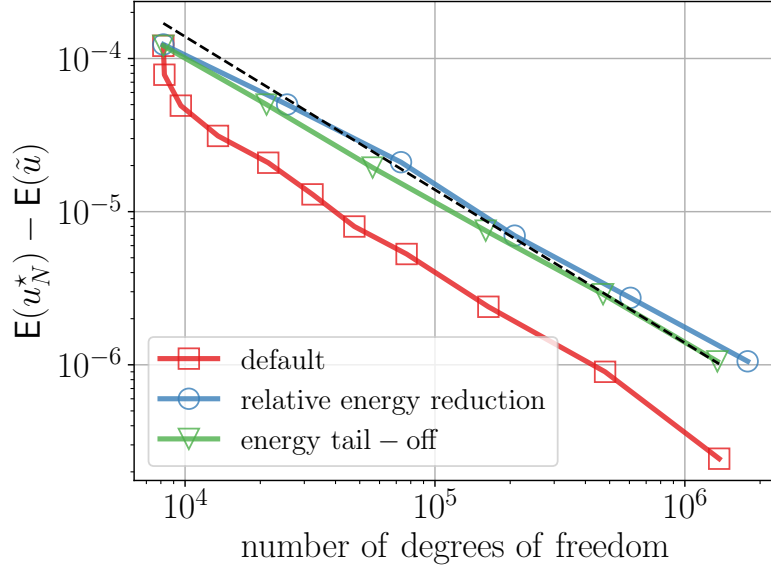


FIGURE 2. Convergence plot for Experiment 1, obtained with Algorithm 3 and three different stopping criteria. The black dashed line represents the optimal convergence rate  $\mathcal{O}(n_{\text{DOF}}^{-1})$ .

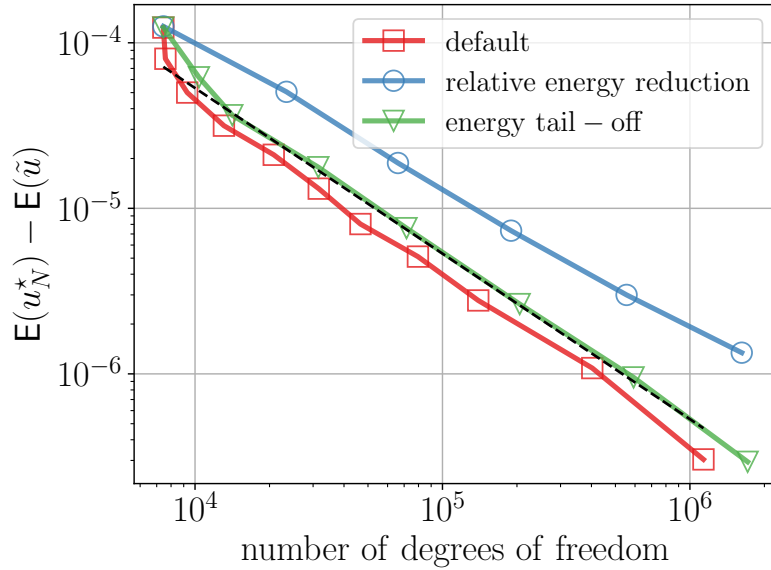


FIGURE 3. Convergence plot for Experiment 2, obtained with Algorithm 3 and three different stopping criteria. The black dashed line represents the optimal convergence rate  $\mathcal{O}(n_{\text{DOF}}^{-1})$ .

*Experiment 3.* In this experiment, we consider the BVP (4.1) with the constant diffusion matrix  $\mathbf{A} := \text{Id}$ , the nonlinearity  $\phi(u) := \exp(u) - 1$ , and the constant right-hand side function  $f := 1$ . The convergence plot in Figure 2 displays results for Algorithm 3 with the following choices of the control parameters for the corresponding stopping criteria. Relative energy reduction:  $\alpha_\gamma = 0.01$ ,  $n_{\min} = 10$ ,  $\tau = 1.001$ ,  $d_{\text{init}} = 50$ ,  $\Delta d = 5$ . Energy tail-off:  $\alpha_E = 0.01$ ,  $n_{\min} = 10$ ,  $n_{\text{batch}} = 5$ . Default:  $n_{\min} = 10$ ,  $g_{\text{tol}} = 10^{-8}$ .

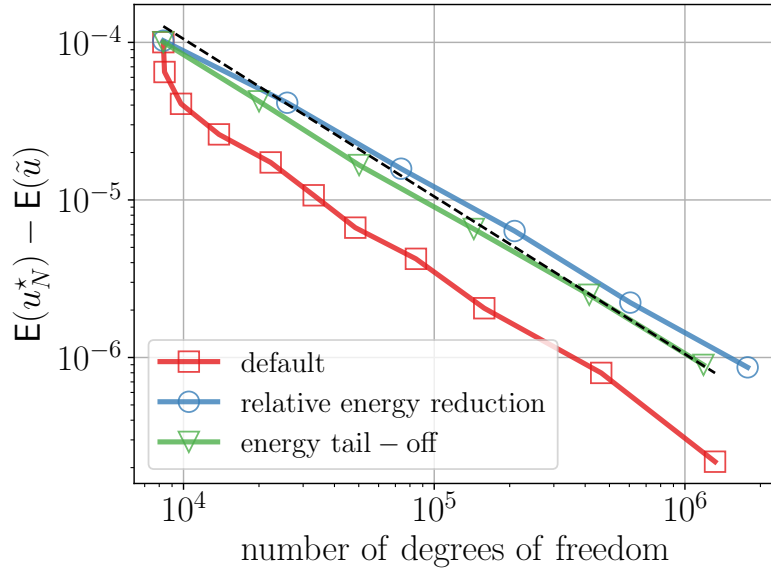


FIGURE 4. Convergence plot for Experiment 3, obtained with Algorithm 3 and three different stopping criteria. The black dashed line represents the optimal convergence rate  $\mathcal{O}(n_{\text{DOF}}^{-1})$ .

Surprisingly, Figure 4 shows almost identical results as we obtained for Experiment 1. Therefore, we again conclude that both the relative energy reduction criterion (2.16) and energy tail-off stopping criterion (2.10) yield optimal convergence behavior, although they are both located about half an order of magnitude above the slope corresponding to the default stopping criterion (2.17).

*Experiment 4.* In this experiment, we consider the BVP (4.1) with the constant diffusion matrix  $\mathbf{A} := \text{Id}$ , and the nonlinearity  $\phi(u) := u^3$ . Further, we choose the right-hand side function  $f$  such that the exact solution is given by the singular function

$$u(x, y) := 2r^{-4/3}xy(1-x^2)(1-y^2),$$

where  $r := \sqrt{x^2 + y^2}$  is the radial distance to the origin. The convergence plot in Figure 2 displays results for Algorithm 3 with the following choices of the control parameters for the corresponding stopping criteria. Relative energy reduction:  $\alpha_\gamma = 0.1$ ,  $n_{\min} = 10$ ,  $\tau = 1.01$ ,  $d_{\text{init}} = 10$ ,  $\Delta d = 5$ . Energy tail-off:  $\alpha_E = 0.01$ ,  $n_{\min} = 10$ ,  $n_{\text{batch}} = 5$ . Default:  $n_{\min} = 10$ ,  $g_{\text{tol}} = 10^{-8}$ .

In Figure 5, we clearly observe that the results obtained with the energy tail-off stopping criterion (2.10) are almost identical to those obtained with the default stopping criterion (2.17). In both cases, the corresponding slopes closely follow the dashed line, indicating optimal convergence behavior. Finally, as already observed in Experiment 2, the slope corresponding to the relative energy decay stopping criterion (2.16) appears to level off slightly once the number of degrees of freedom exceeds a magnitude of  $10^6$ .

**4.2. Linear Experiments.** In this section, we assess Algorithm 3 employed for the numerical solution of (4.1), where we set  $\phi(u) = cu$ , with  $c \in \{0, 1\}$  constant. In this setting, the energy (4.2) reduces to

$$E(v) = \frac{1}{2} \int_{\Omega} \mathbf{A}(\mathbf{x}) \nabla v(\mathbf{x}) \cdot \nabla v(\mathbf{x}) \, d\mathbf{x} + \frac{c}{2} \int_{\Omega} v(\mathbf{x})^2 \, d\mathbf{x} - \int_{\Omega} f(\mathbf{x})v(\mathbf{x}) \, d\mathbf{x},$$

possessing the same structure as the energy in (2.1). As motivated in Section 2.3, the iterative solver, which is employed in this case, is the standard linear CG algorithm provided in `scipy.sparse.linalg.cg`.

We consider four distinct boundary value problems. For each problem, we present numerical results corresponding to both stopping criteria introduced in Section 2.4. The following control

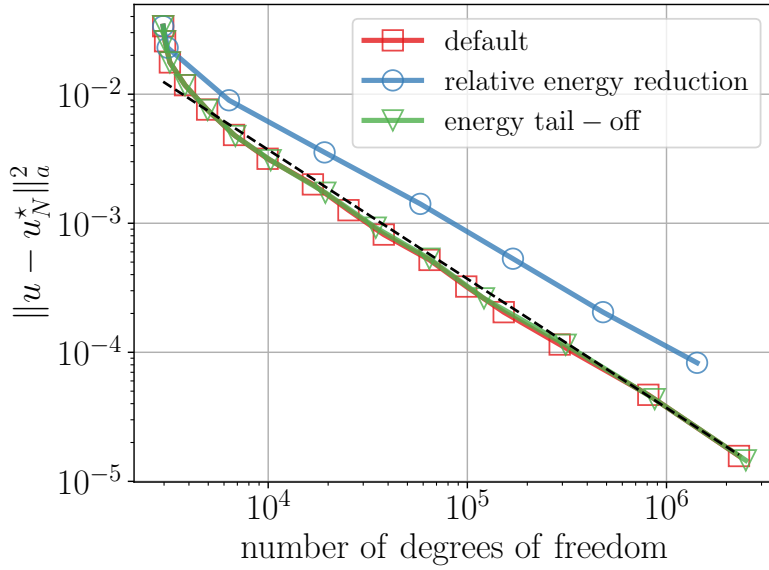


FIGURE 5. Convergence plot for Experiment 4, obtained with Algorithm 3 and three different stopping criteria. The black dashed line represents the optimal convergence rate  $\mathcal{O}(n_{\text{DOF}}^{-1})$ .

parameters are used throughout all experiments:  $\theta = 0.5$ ,  $\alpha_E = 0.1$ ,  $\tau = 1.01$ ,  $d_{\text{init}} = 10$ ,  $\Delta d = 10$ , and  $n_{\text{batch}} = 2$ . All additional control parameters, i.e.  $n_{\text{min}}$  and  $\alpha_\gamma$ , are specifically selected for each experiment, and their choice will be detailed in the respective numerical tests below.

In all experiments, the plots should be read as follows. The line plots with square and circular markers correspond to the vertical axis on the left, representing the energy norm of the errors. In the legend,  $u_N^* \in \mathbb{V}_N$  denotes the final iterate at which the iteration is terminated on the present space, and for which the energy norm of the error is evaluated and plotted. The line plot with triangular markers corresponds to the vertical axis on the right and depicts the number of iterations  $n(N)$  required on each subspace  $\mathbb{V}_N$  before the corresponding stopping criterion terminates the iteration, i.e. we have  $u_N^{n(N)} = u_N^*$ .

*Computational setup.* As the energy is linear-quadratic in this case, the local energy decays in line 5 of Algorithm 2 are computed with (3.10). In the plots corresponding to the experiments below, we report results for the energy norm of both the iteration error  $\|u_N^h - u_N^*\|_a$  and the overall error  $\|u_N^* - u\|_a$ . To compute the energy norm of the iteration error, we compute the Galerkin solution  $u_N^h$  on each mesh using a direct solver. However, to compute the energy norm of the total error  $\|u - u_N^*\|_a$ , we must resort to an approximate procedure, as for all problems considered, the exact full-space solution is unknown. To this end, we exploit (2.4), from which we deduce the useful identity

$$\|u - u_N^*\|_a^2 = 2E(u_N^*) + \|u\|_a^2.$$

The term  $\|u\|_a^2$  is then approximated by a reference value computed on a strongly refined uniform mesh, and its numerical value is provided within the description of each respective experiment below. We note, however, that employing a direct solver to compute the reference value on the final mesh was unfeasible due to memory limitations of the available hardware; therefore, we have resorted to an iterative procedure instead. More precisely, starting from a coarse initial mesh, we perform a sequence of uniform mesh refinements; on each mesh, the CG method is applied with a relative tolerance of  $\epsilon_{\text{rel}} = 10^{-5}$ , that is, until it holds the bound

$$\|\mathbf{b} - \mathbf{A}\mathbf{x}_n\|_2 \leq \epsilon_{\text{rel}}\|\mathbf{b}\|_2,$$

where  $\|\cdot\|_2$  denotes the standard Euclidean norm. The final approximation on each mesh is recycled as initial guess on the corresponding refined mesh, and the final approximation on the finest mesh is used to compute the reference value. For Experiments 5 and 6, this process was continued until the number of degrees of freedom reached a magnitude of  $\dim\mathbb{V}_N \approx 0.30 \cdot 10^8$ , while for Experiment 7, it was stopped at  $\dim\mathbb{V}_N \approx 0.23 \cdot 10^8$ .

We emphasize that all numerical integrations performed in assembling the linear systems in our experiments are carried out exactly. Indeed, for Experiments 5, 6, and 8, this is straightforward since the problem data is constant across the entire domain; in Experiment 7, exact integration is ensured by choosing the initial mesh so that its edges align with the interface boundaries of each subdomain, ensuring the data is constant on each element.

*Experiment 5.* In this experiment, we consider the BVP (4.1) with an anisotropic constant diffusion matrix

$$\mathbf{A}(\mathbf{x}) = \begin{pmatrix} 1 & 0 \\ 0 & 10^{-2} \end{pmatrix},$$

and a constant reaction constant  $c = 1$  on the square domain  $\Omega_S$ . Due to the small diffusion in the second coordinate direction, we expect boundary layers on the top and bottom boundary of  $\Omega_S$  to form in the true solution. To make sure that the convergence is close to optimal already for comparatively small numbers of degrees of freedom, these boundary layers must be resolved rapidly by the adaptive refinement strategy. The energy norm of the true solution is approximated by the reference value

$$\|u\|_a^2 \approx \underline{0.07121857719182778},$$

where, throughout, the underlined part indicates the stable digits in the numerical approximations. From the convergence plots in Figure 6, we observe that the overall error follows the optimal convergence rate for both stopping criteria proposed in Section 2.4. In both cases, the iteration error remains relatively small compared to the total error, thus leading to the conclusion that the discretization error dominates throughout the experiment. Moreover, for either stopping criterion, the number of iterations exhibits a single distinct (comparatively high) outlier, which, indicated by the red line with square markers, appears to ensure that the CG iteration error maintains a certain gap from the total error. Finally, we emphasize that, using our approach, the number of iterations per mesh was reduced by roughly an order of magnitude in comparison with a solution strategy based on uniform mesh refinements combined with the default residual-based stopping criterion of the CG algorithm `scipy.sparse.linalg.cg`; this observation holds true in all of our tests, for which we computed the reference value of the energy norm of the full space solution using the CG algorithm with uniform mesh refinements, i.e. for the current experiment, as well as for the subsequent Experiments 6 and 7.

*Experiment 6.* In this experiment, we consider the BVP (4.1) with a constant diffusion matrix

$$\mathbf{A}(\mathbf{x}) = 10^{-2} \mathbf{1}_{2 \times 2},$$

where  $\mathbf{1}_{2 \times 2}$  denotes the  $2 \times 2$  identity matrix, and a constant reaction coefficient  $c = 1$  on the square domain  $\Omega_S$ . Due to the small (isotropic) diffusion coefficient, we expect boundary layers to form along  $\partial\Omega_S$  in the true solution. As previously in Experiment 5, in order to make sure that the convergence slope attains optimality already for comparatively small numbers of degrees of freedom, these boundary layers must be resolved by the energy-based adaptive refinement strategy. The energy norm of the true solution is approximated by the reference value

$$\|u\|_a^2 \approx \underline{0.6509451171871544}.$$

The convergence plots in Figure 7 indicate that the total error closely follows the optimal convergence behavior. For the energy tail-off stopping criterion (2.10), we observe that the number of linear subspaces considered is visibly higher than in Experiment 5, which is, however, naturally accompanied by a smaller number of iterations per mesh. Moreover, as already observed in Experiment 5, both stopping criteria display a single distinct outlier in the iteration count; this behavior appears to reflect the algorithm's tendency to further reduce the iteration error at certain points, thereby ensuring that it remains sufficiently below the total error.

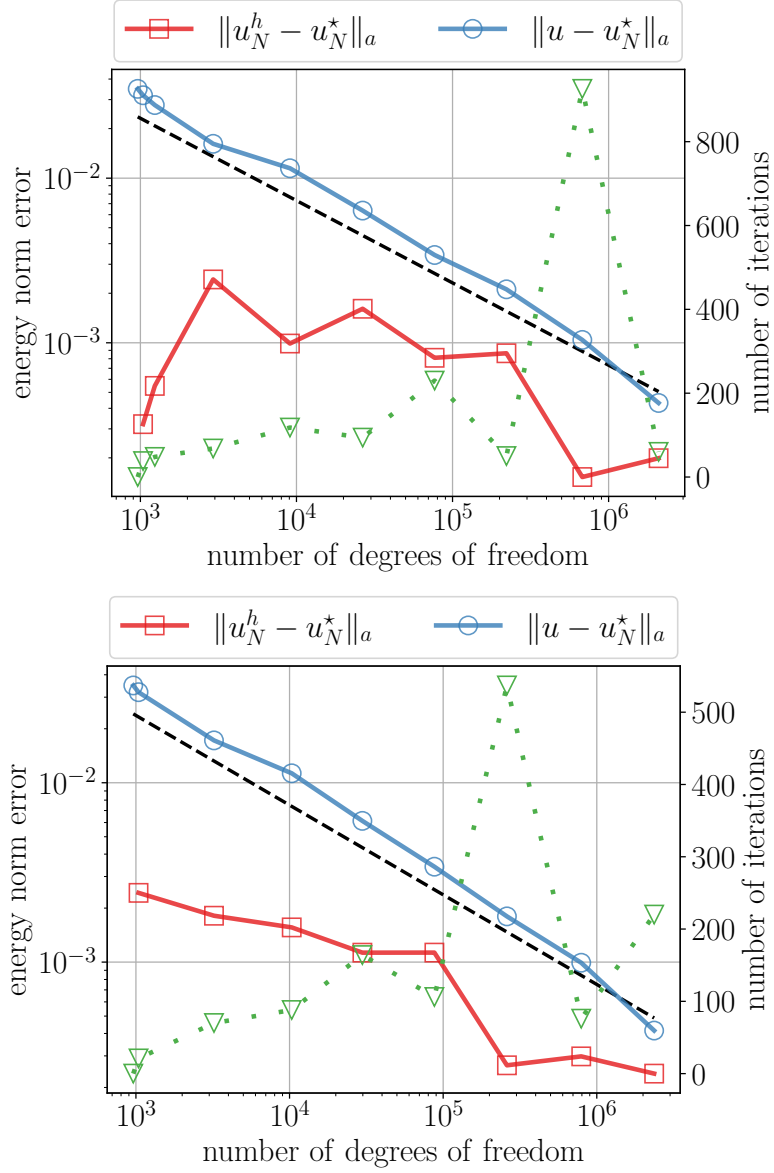


FIGURE 6. Experiment 5. Top: energy tail-off stopping criterion (2.10) with  $n_{\min} = 10$ . Bottom: relative energy reduction stopping criterion (2.14) with  $n_{\min} = 10$ , and  $\alpha_\gamma = 0.1$ .

*Experiment 7.* Here, we consider the BVP (4.1) on the square domain  $\Omega_S$ , with a constant reaction coefficient  $c = 1$ , and a piecewise constant diffusion matrix  $\mathbf{A}(\mathbf{x}) = \kappa(\mathbf{x})\mathbf{1}_{2 \times 2}$ , where

$$\kappa(\mathbf{x}) = \begin{cases} 1, & \mathbf{x} \in \Omega_S \setminus (\Omega_1 \cup \Omega_2 \cup \Omega_3), \\ 10, & \mathbf{x} \in \Omega_1, \\ 0.1, & \mathbf{x} \in \Omega_2, \\ 0.05, & \mathbf{x} \in \Omega_3; \end{cases}$$

the subdomains  $\Omega_1, \Omega_2, \Omega_3 \subset \Omega_S$  are given by

$$\Omega_1 = (0.1, 0.3) \times (0.1, 0.2), \quad \Omega_2 = (0.4, 0.7) \times (0.1, 0.3), \quad \Omega_3 = (0.8, 1.0) \times (0.7, 1.0).$$

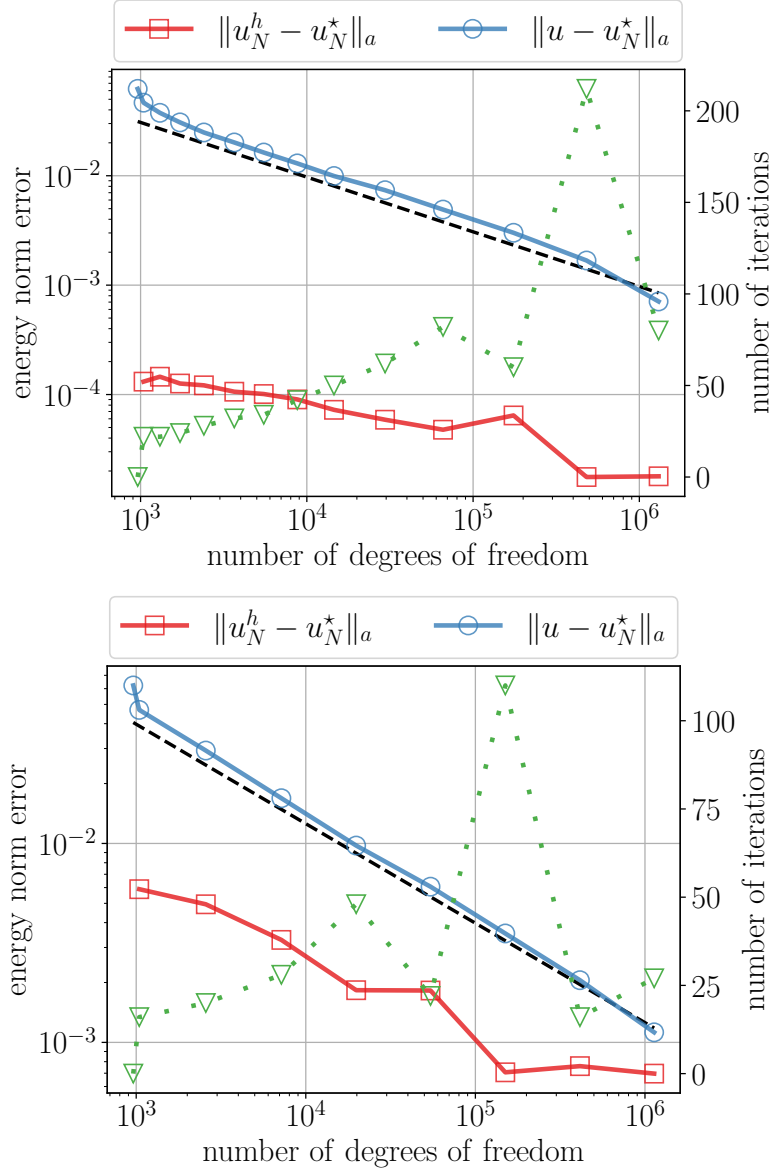


FIGURE 7. Experiment 6. Top: energy tail-off stopping criterion (2.10) with  $n_{\min} = 10$ . Bottom: relative energy reduction stopping criterion (2.14) with  $n_{\min} = 5$ , and  $\alpha_\gamma = 0.1$ .

Since the diffusion matrix has piecewise constant entries that differ by orders of magnitude when switching between subdomains, the interfaces of all subdomains must be adequately resolved by the adaptive refinement strategy; in our computations, the initial mesh has been aligned with the interfaces. In Figure 8 (left), we observe that our adaptive refinement strategy identifies the subdomain corners as particularly important regions to be resolved. Further, we stress that, due to the strongly varying diffusion coefficient, the resulting system is ill-conditioned. Therefore, in this experiment only, we employed the diagonal preconditioner  $\mathbf{P} = \text{diag}(\mathbf{A})^{-1}$ , where  $\mathbf{A}$  denotes the left-hand side matrix in (2.6). This was realized by passing  $\mathbf{P}$  as an additional preconditioning parameter to `scipy.sparse.linalg.cg`. As noted in Remark 2, using any preconditioner does not interfere with the use of our custom stopping criteria. The energy norm of the true solution

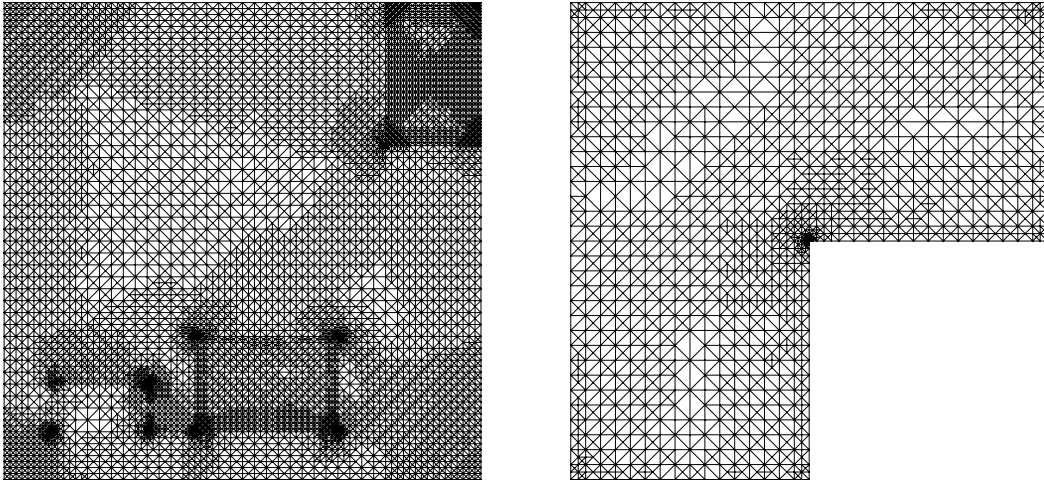


FIGURE 8. Both meshes were obtained in conjunction with the energy tail-off stopping criterion (2.10) and the control parameter  $n_{\min} = 10$ . Left: Adaptively refined mesh for Experiment 7 with 7511 degrees of freedom. Right: Adaptively refined mesh for Experiment 8 with 1330 degrees of freedom.

is approximated by the reference value

$$\|u\|_a^2 \approx 0.04076358619422494.$$

The convergence plots show that the number of linear subspaces generated by the algorithm remains comparatively small for both stopping criteria. At the same time, the number of iterations per mesh stays low, except for the final data point in the case of stopping criterion (2.10), where a higher iteration count reduces the iteration error by roughly one order of magnitude below the total error. In both cases, our energy-based adaptive algorithm is able to attain optimal convergence.

*Experiment 8.* In this test, we consider the BVP (4.1) with a constant diffusion matrix  $\mathbf{A} = \mathbf{1}_{2 \times 2}$ , and a vanishing reaction coefficient  $c = 0$  on the L-shaped domain  $\Omega_L$ . This benchmark problem is well-known to exhibit an elliptic corner singularity at the origin that mandates appropriate local mesh refinement, which is correctly resolved by our adaptive mesh refinement strategy, as can be observed in Figure 8 (right). The energy norm of the true solution is approximated by

$$\|u\|_a^2 \approx 0.214075802220546;$$

this value was obtained<sup>2</sup> by applying a standard *hp*-finite element approach as described in [Sch98, §4]. Our energy-based adaptive refinement strategy successfully identifies the singular behavior in the vicinity of the origin, see Figure 10, thereby ensuring optimal convergence for both stopping criteria of the CG iteration; incidentally, in either case we observe two distinct peaks in the iteration count, which appear to enforce sufficient reduction of the iteration error. As a result, the iteration error remains roughly two orders of magnitude below the total error for the energy tail-off stopping criterion (2.10), and about one order of magnitude below for the relative energy reduction stopping criterion (2.14).

## 5. CONCLUSIONS

We have developed a fully iterative, energy-based adaptive framework for the numerical minimization of strictly convex and weakly coercive energy functionals  $\mathbf{E} : \mathbb{V} \rightarrow \mathbb{R}$  on a Hilbert space  $\mathbb{V}$ .

<sup>2</sup>The authors gratefully acknowledge the help of Dr. Patrick Bammer for carrying out the necessary high-accurate *hp*-FEM computations.

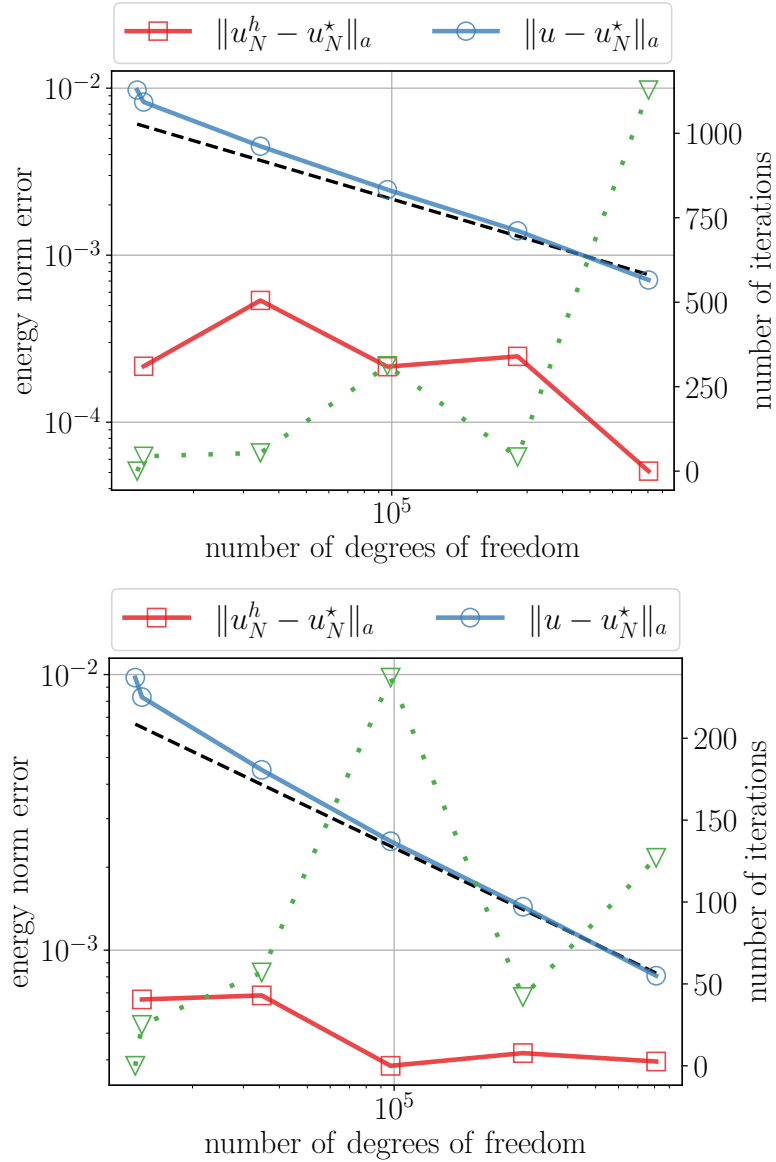


FIGURE 9. Experiment 7. Top: energy tail-off stopping criterion (2.10) with  $n_{\min} = 5$ . Bottom: relative energy reduction stopping criterion (2.14) with  $n_{\min} = 5$ , and  $\alpha_\gamma = 0.1$ .

Roughly speaking, the proposed strategy combines an energy-based adaptive construction of a hierarchical sequence of finite-dimensional subspaces with an iterative energy minimization strategy on each discrete subspace  $\mathbb{V}_N \subset \mathbb{V}$ ,  $N \in \mathbb{N}$ , based on a (nonlinear) CG method in conjunction with energy-based stopping criteria.

Within a more specific framework, we have presented a straightforward realization of our abstract strategy for  $\mathbb{P}_1$  finite element discretizations of the underlying Hilbert space  $\mathbb{V} = H_0^1(\Omega)$ , termed edge-based variational adaptivity. In this context, compared to earlier works, our contribution provides essentially two novelties: Firstly, with respect to adaptive enrichment, previous implementations of *variational adaptivity* compute local energy reductions using element-based refinements, see, e.g., [AHW23; HSW21], whilst in the current work, we exploit the corresponding energy reductions via edge bisection, which are slightly more localized. Secondly, regarding energy

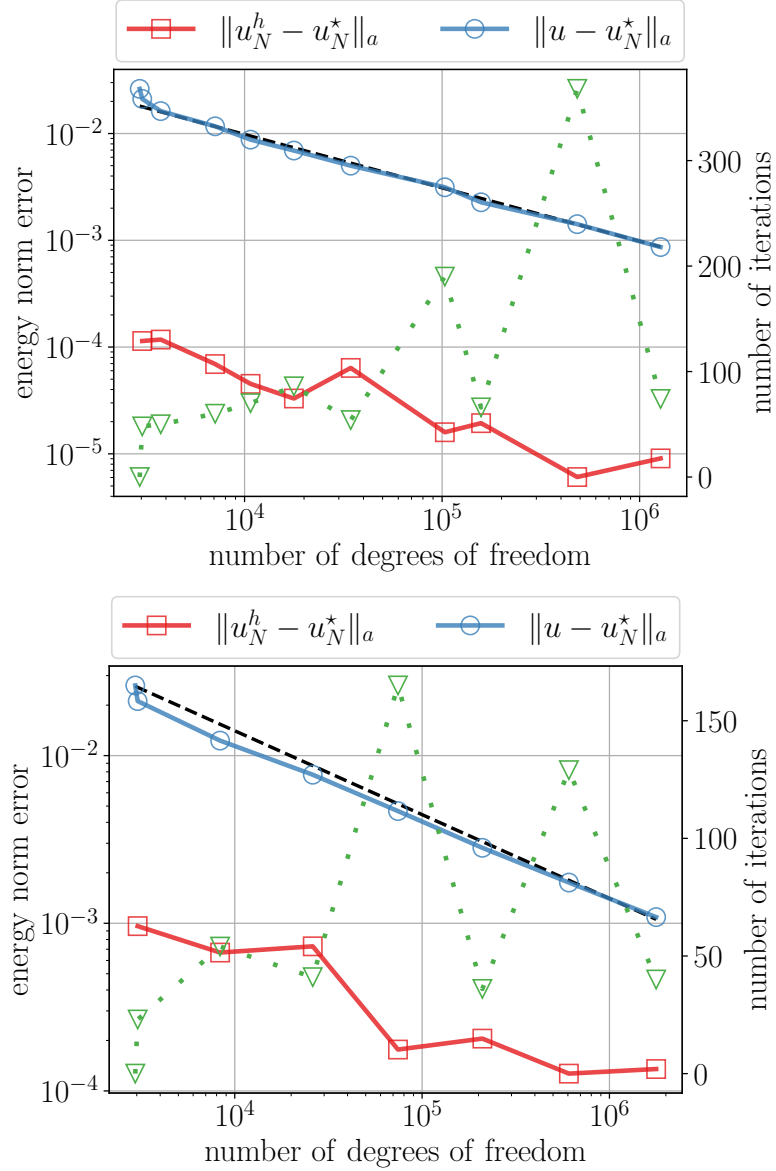


FIGURE 10. Experiment 8. Top: energy tail-off stopping criterion (2.10) with  $n_{\min} = 10$ . Bottom: relative energy reduction stopping criterion (2.14) with  $n_{\min} = 10$ , and  $\alpha_\gamma = 0.01$ .

minimization on each finite-dimensional subspace, our approach intertwines the adaptive space enrichments with a (nonlinear) CG method, again purely based on energy techniques, to solve the discrete minimization problems, and thereby inherently avoids the need to solve any large-scale linear system exactly. Our numerical experiments confirm that, even in this minimal setting of *edge-based variational adaptivity* and without solving any large-scale linear system exactly, the resulting sequence of final iterates  $\{u_N^*\}_N \subset H_0^1(\Omega)$  exhibits optimal convergence rates.

## REFERENCES

- [AHW23] M. Amrein, P. Heid, and T. P. Wihler. “A Numerical Energy Reduction Approach for Semilinear Diffusion-Reaction Boundary Value Problems Based on Steady-State Iterations”. In: *SIAM Journal on Numerical Analysis* 61.2 (Apr. 30, 2023), pp. 755–783.
- [AO00] M. Ainsworth and J. T. Oden. *A posteriori error estimation in finite element analysis*. In collab. with Wiley InterScience (Online service). Pure and applied mathematics. New York: Wiley, 2000. 1 p.
- [Ari04] M. Arioli. “A Stopping Criterion for the Conjugate Gradient Algorithm in a Finite Element Method Framework”. In: *Numerische Mathematik* 97.1 (Mar. 1, 2004), pp. 1–24.
- [Bec+23] R. Becker, M. Brunner, M. Innerberger, J. M. Melenk, and D. Praetorius. “Cost-optimal adaptive iterative linearized FEM for semilinear elliptic PDEs”. In: *ESAIM: M2AN* 57.4 (2023), pp. 2193–2225.
- [BPS25] M. Brunner, D. Praetorius, and J. Streitberger. “Cost-optimal adaptive FEM with linearization and algebraic solver for semilinear elliptic PDEs”. In: *Numerische Mathematik* 157.2 (Apr. 2025), pp. 409–445.
- [BSW25] P. Bammer, A. Schröder, and T. P. Wihler. “An *hp*-Adaptive Strategy Based on Locally Predicted Error Reductions”. In: *Computational Methods in Applied Mathematics* (May 29, 2025).
- [CW17] S. Congreve and T. P. Wihler. “Iterative Galerkin discretizations for strongly monotone problems”. In: *Journal of Computational and Applied Mathematics* 311 (Feb. 2017), pp. 457–472.
- [Dör96] W. Dörfler. “A Convergent Adaptive Algorithm for Poisson’s Equation”. In: *SIAM Journal on Numerical Analysis* 33.3 (June 1996), pp. 1106–1124.
- [EV13] A. Ern and M. Vohralík. “Adaptive inexact Newton methods with a posteriori stopping criteria for nonlinear diffusion PDEs”. In: *SIAM Journal on Scientific Computing* 35.4 (2013), A1761–A1791.
- [FPW11] S. Funken, D. Praetorius, and P. Wissgott. “Efficient implementation of adaptive P1-FEM in Matlab”. In: *Computational Methods in Applied Mathematics* 11.4 (Jan. 1, 2011). Publisher: De Gruyter, pp. 460–490.
- [Glo84] R. Glowinski. *Numerical Methods for Nonlinear Variational Problems*. Berlin, Heidelberg: Springer Berlin Heidelberg, 1984.
- [Hab+21] A. Haberl, D. Praetorius, S. Schimanko, and M. Vohralík. “Convergence and quasi-optimal cost of adaptive algorithms for nonlinear operators including iterative linearization and algebraic solver”. In: *Numerische Mathematik* 147.3 (2021), pp. 679–725.
- [Har+24] A. Harnist, K. Mitra, A. Rappaport, and M. Vohralík. *Robust augmented energy a posteriori estimates for Lipschitz and strongly monotone elliptic problems*. 2024. eprint: HAL04033438.
- [Hei+25] P. Heid, P. Houston, B. Stamm, and T. P. Wihler. *Gradient Flow Finite Element Discretisations with Energy-Based  $\mathcal{H}^1$ -Adaptivity for the Gross-Pitaevskii Equation with Angular Momentum*. Dec. 18, 2025. arXiv: 2412.17680 [math].
- [HPW21] P. Heid, D. Praetorius, and T. P. Wihler. “Energy Contraction and Optimal Convergence of Adaptive Iterative Linearized Finite Element Methods”. In: *Computational Methods in Applied Mathematics* 21.2 (Apr. 1, 2021), pp. 407–422.
- [HS52] M. Hestenes and E. Stiefel. “Methods of conjugate gradients for solving linear systems”. In: *Journal of Research of the National Bureau of Standards* 49.6 (Dec. 1952), p. 409.
- [HSW21] P. Heid, B. Stamm, and T. P. Wihler. “Gradient flow finite element discretizations with energy-based adaptivity for the Gross-Pitaevskii equation”. In: *Journal of Computational Physics* 436 (July 1, 2021), p. 110165.

- [HW20] P. Heid and T. Wihler. “Adaptive iterative linearization Galerkin methods for nonlinear problems”. In: *Mathematics of Computation* 89.326 (July 7, 2020), pp. 2707–2734.
- [HW25] P. Heid and T. P. Wihler. *Iterative energy reduction Galerkin methods and variational adaptivity*. 2025. arXiv: 2509.09600 [math.NA].
- [HZ06] W. W. Hager and H. Zhang. “A survey of nonlinear conjugate gradient methods”. In: *Pacific Journal of Optimization* 2 (Jan. 2006).
- [JSV10] P. Jiránek, Z. Strakoš, and M. Vohralík. “A Posteriori Error Estimates Including Algebraic Error and Stopping Criteria for Iterative Solvers”. In: *SIAM Journal on Scientific Computing* 32.3 (2010), pp. 1567–1590. eprint: <https://doi.org/10.1137/08073706X>.
- [MT24] G. Meurant and P. Tichý. *Error Norm Estimation in the Conjugate Gradient Algorithm*. Philadelphia, PA: Society for Industrial and Applied Mathematics, 2024. eprint: <https://epubs.siam.org/doi/pdf/10.1137/1.9781611977868>.
- [NW06] J. Nocedal and S. J. Wright. *Numerical optimization*. Second edition. Springer series in operations research and financial engineering. New York, NY: Springer, 2006. 1 p.
- [Sch98] C. Schwab. *p- and hp-finite element methods: theory and applications in solid and fluid mechanics*. Numerical mathematics and scientific computation. Oxford Oxford New York: Clarendon Press Oxford university press, 1998.
- [SW25] F. Spicher and T. P. Wihler. *Optimal finite element approximations of monotone semilinear elliptic PDE with subcritical nonlinearities*. 2025. arXiv: 2504.11292 [math.NA].
- [Vir+20] P. Virtanen et al. “SciPy 1.0: Fundamental Algorithms for Scientific Computing in Python”. In: *Nature Methods* 17 (2020), pp. 261–272.
- [Zei90] E. Zeidler. *Nonlinear functional analysis and its applications. II/B*. Nonlinear monotone operators, Translated from the German by the author and Leo F. Boron. Springer-Verlag, New York, 1990, i–xvi and 469–1202.